Relating the circadian dynamics of cortical glutamate to human motor plasticity: a trimodal MRS-EEG-fMRI imaging study

Kiana Ezzatdoost

A Thesis

in

The Department

of

Electrical and Computer Engineering

Presented in Partial Fulfillment of the Requirements

for the Degree of

Master of Applied Science (Electrical and Computer Engineering) at

Concordia University

Montreal, Quebec, Canada

December 2023

CONCORDIA UNIVERSITY

School of Graduate Studies

This is to certify that the thesis prepared

By: **Kiana Ezzatdoost**

Entitled: **Relating the circadian dynamics of cortical glutamate to human motor plasticity: a trimodal MRS-EEG-fMRI imaging study**

and submitted in partial fulfillment of the requirements for the degree of

Master of Applied Science (Electrical and Computer Engineering)

complies with the regulations of the University and meets the accepted standards with respect to originality and quality.

Signed by the final Examining Committee:

_____ Chair

Dr. Hassan Rivaz

_____ Examiner

Dr. Christophe Grova

_____ Examiner

Dr. Julien Doyon

_____ Supervisor

Dr. Habib Benali

Approved by _____

Dr. M. Zahangir Kabir, Graduate Program Director

January, 2023 _____

Dr. Mourad Debbabi, Dean Faculty of Engineering and Computer Science

ABSTRACT

Relating the circadian dynamics of cortical glutamate to human motor plasticity: a trimodal MRS-EEG-fMRI imaging study

Kiana Ezzatdoost

Performing voluntary motor actions, ranging from basic movements such as walking to more complex movements like playing piano, is an integral part of our daily life. Understanding the underlying mechanism of motor learning can benefit education, sports training, and clinical rehabilitation. This study aims to investigate motor learning using diurnal variation in glutamate concentration, the main excitatory neurotransmitter in the central nervous system. To do so, glutamate concentration was measured by magnetic resonance spectroscopy (MRS) at several time points during a control visit and an MSL visit, which employed a finger-tapping sequence task. The study focused on two regions of interest: the supplementary motor area (SMA) as a motor-implicated region and the posterior cingulate cortex (PCC) as a control region.

Electroencephalogram (EEG) and functional magnetic resonance imaging (fMRI) techniques were used alongside MRS to comprehensively track the underlying neuronal mechanism that facilitates learning.

The finding of this study suggests that neuronal plasticity and the creation of memory traces rely on the modulation of glutamate concentrations, specifically in the motor-implicated area. Additionally, the results reveal a tight coupling between metabolism, cerebral blood flow, and neuronal activity, indicating the necessity of employing multi-modal imaging studies to explore learning-induced processes.

Acknowledgments

I would like to express my sincere gratitude to my supervisor, Dr. Habib Benali, for his guidance, mentorship, and support throughout the completion of my master's thesis. His expertise and invaluable insights have been instrumental in shaping the path of my research journey.

Furthermore, I would like to express my heartfelt appreciation to my spouse, Amirsina Nassirian, and my family. Their unwavering support, understanding, and encouragement have been my pillars of strength. Their belief in my abilities and their sacrifices to create a helpful environment for my academic pursuits have been crucial elements contributing to my success.

Finally, I would like to convey my deep appreciation to my colleague, Pierre Berrior, for his collaborative spirit, engagement, and dedication. Collaborating with him has significantly enriched my research experience, and I am thankful for his support.

Table of contents

List of figures vii
List of tables ix
Chapter 1 : Introduction 1
1.1 Background 1
1.2 Problem statement 2
1.3 Objectives 2
1.4 Thesis organization 3
Chapter 2 : Theoretical groundwork 4
2.1 Learning 4
2.1.1 Explicit vs implicit learning 4
2.1.2 Learning phases 5
2.2 Glutamate as a marker 6
2.2.1 Neuroplasticity and synaptic transmission 6
2.2.2 Energy metabolism 8
2.3 Circadian rhythm 9
2.3.1 Sleep-wake cycle 9
2.3.2 Memory consolidation 11
2.4 Neural oscillation 12
Chapter 3 : Methodology 15
3.1 Experimental procedure 15
3.1.1 Task design 17
3.1.2 Sample size 18
3.1.3 Inclusion criteria 19
3.2 Data acquisition 19
3.2.1 Magnetic Resonance Spectroscopy (MRS) 20
3.2.2 Electroencephalogram (EEG): 23
3.2.3 Functional magnetic resonance imaging (fMRI): 27
Chapter 4 : Data analysis 28
3.1 MRS data analysis 28
3.1.1 Preprocessing 28
3.1.2 Fitting 30

3.1.3 Quantification 31
3.2 MRS software 31
3.2.3 FSL-MRS 33
3.3 EEG data analysis 34
3.3.1 Preprocessing 35
3.3.2 Band power analysis 36
3.4 Functional MRI data analysis 37
3.4.1 Preprocessing 37
3.4.2 Extraction of bold time series: 41
3.5 Statistical analysis 42
3.5.1 Shapiro-Wilk test 42
3.5.2 Wilcoxon Signed-Rank test: 43
3.5.3 Friedman test: 43
3.5.4 Bootstrap method: 44
Chapter 5 : Results and discussion 45
5.1 MRS results (first approach): 46
5.1.1 FID-A preprocessing results: 46
5.1.2 Tarquin fitting results: 47
5.2 MRS results (second approach): 48
5.3 Subject-level analysis 50
5.3.1 Diurnal changes in glutamate levels: 50
5.3.2 EEG analysis: 52
5.3.3 Functional MRI BOLD signal: 54
5.4 Group-level analysis 55
5.4.1 Performance duration: 55
5.4.2 Average glutamate changes: 56
Chapter 6 : Conclusions and future work 59
6.1 Concluding remarks 59
6.2 Future work 60
References 61

List of figures

Figure 2.1: Different types of memories. 5
Figure 2.2: Performance enhancement during different stages of motor acquisition including fast learning, consolidation, and slow learning. 6
Figure 2.3: Glutamate journey in the extracellular space. 8
Figure 2.4: The homeostasis hypothesis by Tononi and Cirelli 10
Figure 2.5: Skill acquisition process involving encoding, consolidation, reactivation, and reconsolidation. 13
Figure 3.1: Study design including six data collection throughout the waking period, specifically at 9:00, 11:00, 13:00, 17:00, 21:00 and then again at 9:00 on the following day. 17
Figure 3.2: Task design 18
Figure 3.3: a) The MRI scanner at Perform Centre. b) Our setup inside the scanner. 20
Figure 3.4: An MR spectrum showing peaks for Glutamate (GLU), Total Creatine (tCr), Myo-inositol (Ins), Glyceryl phosphorylcholine (GPC), Total N-acetyl aspartic acid, and Macromolecules at 0.9 ppm (MM09). 21
Figure 3.5: Regions of interest: a) Supplementary motor area (SMA). b) Posterior cingulate cortex (PCC). 23
Figure 3.6: An EEG signal showing waveforms of 32 channels. 24
Figure 3.7: The 10-20 system employed for electrode placement, utilizing only the 32 darker channels, with AFz and FCz serving as the ground and reference, respectively. 25
Figure 3.8: EEG setup 25
Figure 3.9: EEG-fMRI configuration 26
Figure 3.10: A raw fMRI sample 27
Figure 4.1: Tarquin GUI interface 32
Figure 4.2: Tarquin's sample fit 33
Figure 4.3: FSL MRS sample fit 34
Figure 4.4: a) raw EEG data acquired simultaneously with fMRI. b) Pulse artifact corrected EEG 36
Figure 4.5: Power spectral density (PSD) samples 37
Figure 4.6: Estimated transformation for motion correction 38
Figure 4.7: Slice timing correction 39

Figure 4.8: SMA labelled mask. 41
Figure 5.1: Signals before and after coil combination (Subject02/MSL day/ Session2/SMA region). a) Signals received by different coils at distinct locations with reference to the voxel of interest. b) Signals after applying the appropriate complex weights. 46
Figure 5.2: Preprocessing results obtained by aligning and averaging the spectra. 47
Figure 5.3: The fitting results (red curve) with the contribution of glutamate (green curve) for two subsequent sessions. a) Subject05/MSL day/Session2/SMA region. b) Subject05/MSL day/Session3/SMA region 48
Figure 5.4: Coil combination in FSL-MRS (Subject02/MSL day/ Session2/SMA region). 48
Figure 5.5: Aligning and averaging the spectra by FSL-MRS (Subject02/MSL day/ Session2/SMA region). 49
Figure 5.6: Residual water peak removal using HLSVD algorithm in FSL-MRS (Subject02/MSL day/ Session2/SMA region). 49
Figure 5.7: Diurnal glutamate variation on the MSL and control day (Subject01). a) PCC region. b) SMA region. 50
Figure 5.8: Cortisol concentration measurements for Subject01 (MSL visit) 51
Figure 5.9: Melatonin concentration measurements on the MSL and control day for Subject01 52
Figure 5.10: Average beta band power for Subject01. 53
Figure 5.11: Average gamma band power for Subject01. 53
Figure 5.12: Area under the curve (AUC) for BOLD signal on the MSL and control day (Subject01). 54
Figure 5.13: Performance duration for each MSL task session. 56
Figure 5.14: Group averaged glutamate concentrations in SMA and PCC 57
Figure 5.15: Glutamate concentration on MSL day normalized with respect to the control day. 58

List of tables

Table 1: Tarquin's input parameters..... 33

Chapter 1 : Introduction

This chapter introduces the fundamental components of the thesis offering a concise overview of the background knowledge, the necessity of the conducted study, its aims and objectives, and the overall organization of the thesis.

1.1 Background

A wide range of our daily activities, from simple actions such as dialling a phone number to more complex skills like playing a musical instrument, involves performing a series of interlinked movements. Performing such a sequence of movements is composed of planning and execution of each element in the sequence requiring the integration of several cognitive processes. Understanding how memories of these new motor actions are formed is a central endeavour of contemporary neuroscience.

Any new motor skill can be learned by practice.

Through repetition, a motor sequence can be performed more accurately and more rapidly. Learning a motor sequence can be divided into three different stages, including a fast learning phase within the first sessions, a consolidation phase where learning becomes stable, and a slow between-session performance improvement [1]. The underlying reason for the mentioned performance improvement is that the brain, as one of the most complex organs in our body, will undergo noticeable functional and structural alternations to optimize the sequence implementation. These changes demonstrate the nervous system's ability to adjust according to its environment and it’s known as neural plasticity [2]. In more depth, neural plasticity reflects the cellular-related processes of learning. Glutamate, the most abundant excitatory neurotransmitter in the central nervous system (CNS), plays a direct role in inducing long-term potentiation (LTP) through its AMPA and NMDA receptors [3].

During different phases of learning, the metabolic demand of involved areas is expected to vary, and astrocytes, as the main glial cells in CNS, are in charge of fueling this metabolism alternation [4], [5]. As a part of the mentioned neurometabolic coupling, stimulated neurons will release glutamate in the extra-cellular space. Astrocytes consume glutamate to trigger glucose metabolism producing lactate as a byproduct. In the end, neurons can uptake the released lactate to meet their energy demands [6].

The present neurometabolic coupling proves that encoding, storage, and retrieval of motor skill learning is not solely dependent on neurons [7]. Hence, alongside neuronal activity, metabolic processes should also be taken into account while studying the corresponding learning.

1.2 Problem statement

Several studies have been done to explore motor learning in animals and humans. These studies have provided valuable insights into fundamental aspects of different types of motor learning, including the underlying neural mechanism [2], [8], cognitive processes [9], [10], the role of specific brain regions [11], [12], and the effect of diseases or injuries [13], [14].

The present literature has mainly focused either on the neuronal activity of the brain or the metabolic correlates of learning-induced plasticity, neglecting the definite bind between them. To fully understand the complex process of learning a motor skill in humans, a comprehensive study needs to be done including different stages of skill acquisition as the learning progresses. In addition to covering a broad learning time span, the inevitable neurometabolic coupling raises the need for a multi-modal study, which simultaneously investigates the neuronal and metabolic activity of the brain. Conventional techniques such as electroencephalogram (EEG) and functional magnetic resonance imaging (fMRI) may be used for tracking the neuronal activity of the brain. However, to evaluate the metabolic processes, a metabolite marker needs to be determined before recording the concentration of metabolites using magnetic resonance spectroscopy (MRS). Glutamate is the primary excitatory neurotransmitter in the CNS, which plays a fundamental role in synaptic transmission and neuronal plasticity [15]. Consequently, it would serve as a suitable marker for inspecting various stages of learning.

1.3 Objectives

The objectives of this experiment can be divided into two parts:

1) Data acquisition:

The initial phase of the project involved designing and implementing an experimental protocol to investigate dynamic variations in glutamate and neuronal activity induced by a motor sequence learning task. This protocol also involved a control condition that did not involve learning and was only utilized for comparison analysis. This phase aimed to employ three different imaging techniques,

including MRS, EEG, and fMRI to capture the neurometabolic trace of motor learning.

2) Data analysis:

The latter phase of the study was centred on constructing a framework for analyzing the obtained data in order to facilitate further interpretation of the results. During this phase, the raw data from different modalities were preprocessed and processed by custom-designed scripts which utilized relevant software.

Ultimately, the main goal is to reveal and model the link between glutamate variation and mastering a motor sequence. Meanwhile, the contribution of neuronal activity will be recorded for a more comprehensive investigation. To fulfill this purpose, data from healthy participants who met our inclusion criteria were collected and processed, primarily focusing on two regions of interest: the supplementary motor area (SMA) and the posterior cingulate cortex (PCC).

1.4 Thesis organization

This thesis is organized into six chapters, each covering a unique aspect of the subject. The rest of the thesis is structured as follows:

- Chapter 2 (Literature review): This chapter establishes the theoretical groundwork of the study by discussing the theoretical aspects and the relevant literature.
- Chapter 3 (Methodology): This chapter presents the methodology, providing a detailed explanation of the experimental procedures, data acquisition, and each imaging technique.
- Chapter 4 (Data Analysis): This chapter introduces the data processing framework for each modality along with the utilized software and the implemented statistical analysis.
- Chapter 5 (Results): This chapter presents data processing and statistical analysis results. It also includes a detailed discussion of our hypotheses and interpretation of the results.
- Chapter 6 (Conclusions and future works): This chapter summarizes the main discussion on the findings of the experiment and defines a path for future works.

Chapter 2 : Theoretical groundwork

After covering the primary aspects of this study in chapter one, this chapter is supposed to provide a theoretical foundation for the proposed experiment.

2.1 Learning

2.1.1 Explicit vs implicit learning

Any learning can occur either implicitly or explicitly (Figure 2.1). Implicit motor sequence learning refers to cases where individuals don't have a conscious awareness of the learning occurrence or what has been learned. Whereas explicit motor sequence learning involves a conscious effort to learn and improve the performance of a sequence with an explicitly known structure.

The latter is known to depend on declarative memory which is categorized into semantic and episodic memory. Declarative memory is the memory of facts (semantic memory) and events (episodic memory) often described as a "what" memory (e.g., remembering last night's dinner) [16]. Explicit learning is often associated with a more rapid pace in skill acquisition as it profits from intentional attention. On the other hand, in the former type of learning, performance improvement gradually happens through repeated practice. Implicit motor learning is known to engage procedural memory which involves unconscious retrieval of information on how to do things (e.g., riding a bike) [17].

There has been a controversial debate in the literature regarding the underlying neural processes in implicit versus explicit learning. Some studies have reported the parietal to premotor area (dorsal stream) involvement in implicit learning in contrast to the prefrontal cortex to the posterior temporal lobe (ventral stream) engagement in explicit learning [18]. Some other studies suggest ventral stream can be shared by explicit and implicit learning [19]. Lastly, few studies have proposed a shared neural substrate at which the implicit learning process originates from the motor cortex, leading to the premotor and prefrontal cortex whereas the process in explicit sequence learning begins from the prefrontal cortex, moving to premotor and motor regions [20], [21]. More recent imaging studies also confirm the contribution of SMA, primary motor cortex, prefrontal cortex, and striatum in implicit learning [22]. These studies present an alternative perspective to implicit/explicit learning, in which motor learning is known to be facilitated by explicit knowledge

in the early stages and executed automatically or implicitly in the final stages [1]. From the other perspective, implicit sequence learning refers to the lack of awareness regarding the repetitive pattern hidden within the implemented sequence, rather than being unaware of the sequence itself. With this definition, subjects may develop an explicit knowledge of the sequence as learning progresses [20].

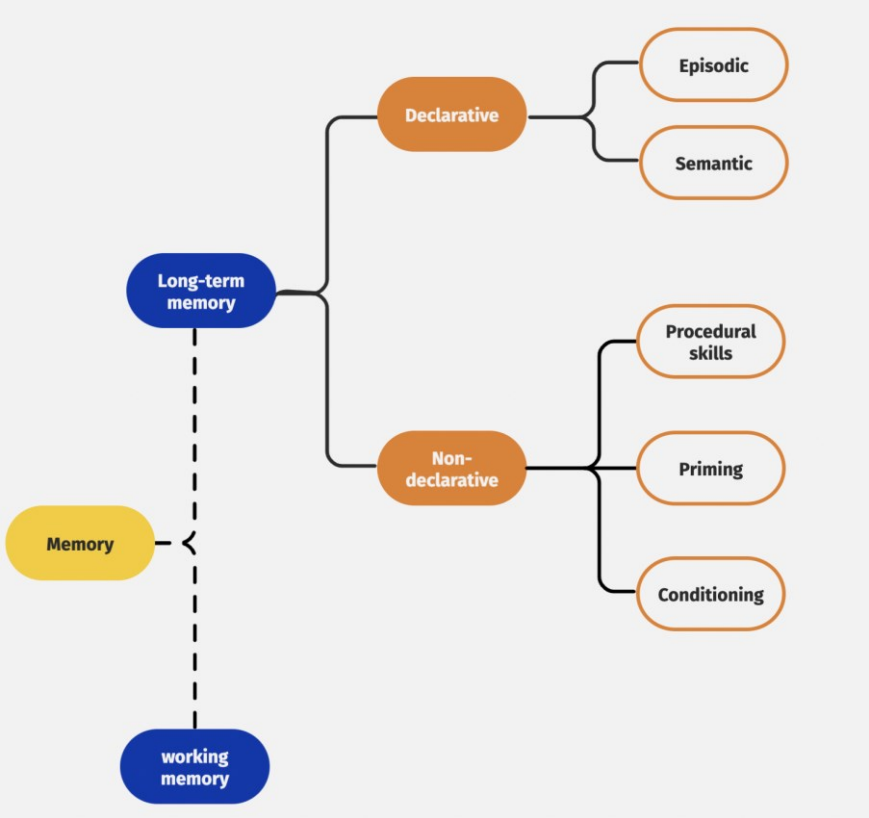

Figure 2.1: Different types of memories.

Nonetheless, implicit learning is crucial for a broad range of our abilities. It can be impaired by different kinds of brain damage, such as Parkinson's disease, cerebellar disease, and brain lesions caused by stroke or injury [14]. Therefore, it is essential to further investigate and understand this learning mechanism to leverage it in education, sports training, and clinical rehabilitation.

2.1.2 Learning phases

A motor skill is acquired in different stages (Figure 2.2). Initially, a fast within-session performance improvement is observed, which depending on the skill's type and complexity can

make up most of our performance. This stage is followed by slow across-session learning which further improves the performance. There is also an intermediate phase between sessions and during the rest period where the acquired skill becomes resistant to interference or time passage. This phase is known as the consolidation phase [23]. The late phase of learning is mainly associated with chunking the sequence and encoding its motor components while the early phase is known to deal with spatial components [20].

Although several experiments were conducted to study motor sequence learning, only a few of them have explored skill acquisition during all different stages of it. The lack of sufficient literature in this area raises the need for a comprehensive study tracking motor learning in different stages over time.

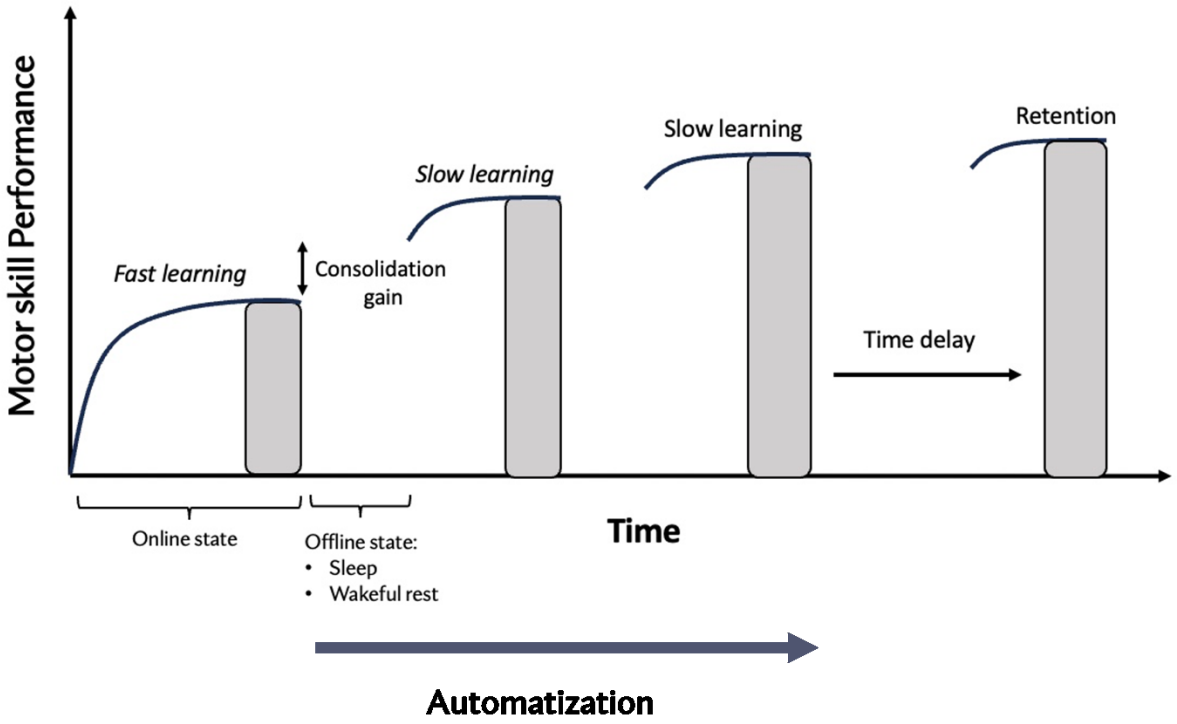

Figure 2.2: Performance enhancement during different stages of motor acquisition including fast learning, consolidation, and slow learning.

2.2 Glutamate as a marker

2.2.1 Neuroplasticity and synaptic transmission

Now that we have reviewed different types and phases of learning, we should go beyond the

surface level to explore the molecular origin of learning.

Neuroplasticity refers to the central nervous system's (CNS) ability to reorganize its function or structure in response to behavioural or environmental changes. Learning a new sequence depends on long-term potentiation (LTP). LTP is a well-known form of long-term plasticity, characterized by a lasting increase in synaptic efficacy resulting from persistent stimulation [24]. During LTP, neural circuits are rewired by changing the strength of existing synaptic connections or by adding/removing some connections. This alteration in synaptic transmission is known to contribute to the encoding and storage of learning information in the brain. Comprehensive animal studies also validate the contribution of postsynaptic potentiation in the memory representation of motor learning [25].

Glutamate is the main excitatory neurotransmitter in CNS that plays a fundamental role in synaptic transmission and the abovementioned synaptic plasticity. Glutamate binds to ionotropic and metabotropic receptors on the postsynaptic membrane. Ionotropic receptors are directly linked to ion channels. When glutamate binds to these receptors, the ion channels open, leading to changes in the membrane potential and the flow of ions across the membrane (Figure 2.3). By binding to ionotropic receptors, glutamate depolarizes the postsynaptic neuron. With sufficient magnitude, this depolarization can lead to the generation of an action potential and transmission of signals from one neuron to another. In contrast, metabotropic receptors are known to impact postsynaptic neurons through specific G-proteins [26].

Glutamate is also involved in synaptic plasticity by acting on two types of ionotropic receptors: AMPA (α-amino-3-hydroxy-5-methyl-4-isoxazolepropionic acid) and NMDA (N-methyl-D-aspartate) receptors. During LTP induction, the initial activation of AMPA receptors leads to the influx of Na+ depolarizing the postsynaptic membrane. Subsequently, NMDA receptors become engaged allowing Ca^{2+} to enter the postsynaptic neuron. This increase in intracellular Ca^{2+} concentration triggers a cascade of molecular events, activating various kinases, including CaMKII (calcium/calmodulin-dependent protein kinase II). CaMKII phosphorylates AMPA receptors leading to their increased conductance and insertion into the postsynaptic membrane (Figure 2.3). This mechanism results in an enduring increase in synaptic strength, reflecting LTP's underlying molecular processes [27], [28]. The mentioned calcium influx can also activate signalling pathways that influence dendritic spine morphology [29], [30].

2.2.2 *Energy metabolism*

Another role of glutamate is to regulate energy metabolism through glutamate-driven glycolysis. After neurons release glutamate during synaptic transmission, astrocytes, the primary glial cells in the CNS, clear up glutamate from the synaptic cleft. This glutamate uptake stimulates glycolysis which is a metabolic pathway where glucose is broken down to produce energy [31]. While learning a new sequence of motor actions, the energy demand of activated areas in the brain will rise following the tight integration of synaptic transmission and energy metabolism. The process of providing the neurons with their energy demand is indirectly dependent on glutamate. Because of glutamate involvement in both neuronal stimulation and metabolite regulation, it would be an excellent biochemical marker for comprehensive studies dealing with neurometabolic coupling.

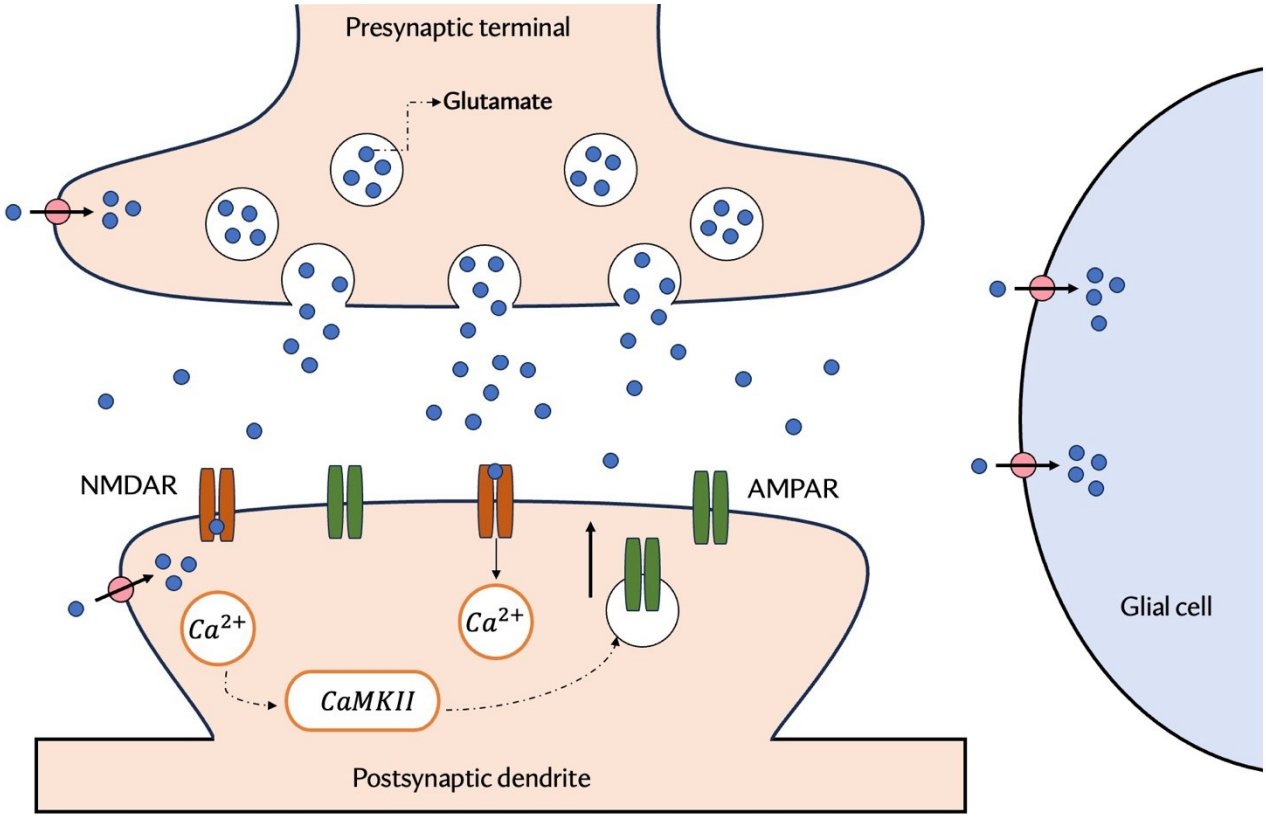

Figure 2.3: Glutamate journey in the extracellular space.

2.3 Circadian rhythm

The circadian rhythm is a naturally occurring, roughly 24-hour cycle that regulates various physiological and metabolic processes, including those within the human brain. At the cellular level, the circadian rhythm of each tissue is controlled by a group of genes called clock genes. At the higher level, there is a master pacemaker located in the suprachiasmatic nucleus (SCN) of the hypothalamus that integrates external information, such as the light-dark cycle from the eyes, and synchronizes these cellular rhythms accordingly [32]. This biological clock impacts crucial processes for a healthy, including the sleep-wake cycle influenced by melatonin release, fluctuations in neurotransmitter levels such as serotonin, dopamine, and glutamate, hormonal regulation with cortisol exhibiting circadian peaks, temperature variations impacting metabolic functions, and the temporal coordination of gene expression. This influence extends to learning, cognitive functions, and memory.

Disrupting the circadian rhythm can have serious health risks. Sleep disorders, including insomnia and irregular sleep patterns, are common consequences of circadian disruption [33]. Cognitive function may be impaired, leading to difficulties in learning and memory [34]. Mood disorders, such as an increased risk of depression and anxiety, can result from irregular circadian rhythms [35]. Metabolic dysregulation, including obesity and insulin resistance, and cardiovascular problems are other potential outcomes of a disturbed circadian rhythm [36], [37]. Cardiovascular problems and a higher risk of certain cancers are also linked to long-term circadian disruption [38]. Maintaining a regular sleep-wake routine which is synchronized with the natural light-dark cycle is important for avoiding these adverse effects [39].

The present literature suggests that the function of glutamate transporters, a type of protein that helps astrocytes take up the excess glutamate from the synaptic cleft, could also be regulated in a diurnal and circadian manner [40], [41]. Therefore, in longitudinal studies on glutamate dynamic variation, it is crucial to only include participants with well-synchronized sleep-wake cycles.

2.3.1 Sleep-wake cycle

The influence of sleep on healthy brain function is inevitable. Although the exact mechanism of sleep has not been fully understood yet, the restorative nature of sleep is known to be associated with sleep homeostasis. The sleep homeostasis hypothesis (SHY), first proposed by Tononi and Cirelli, suggests that sleep alleviates the plasticity pressure on neurons and cells by regulating synaptic strength, ultimately restoring neurons' selectivity and ability to learn [39]–[41] (Figure

2.4). Throughout periods of wakefulness, we consistently face different stimuli leading to the accumulation of synaptic strength. Besides, the learning and development of a new skill will also trigger synaptic plasticity and synaptogenesis. Increased synaptic plasticity comes at a price. Greater energy consumption, an increased need for cellular resources to be delivered to synapses, resulting in cellular stress, and related alterations in support cells like glia are some of the costs associated with increased synaptic strength. In addition, the neuron's selectivity may be diminished as it will become more sensitive to a wider range of input patterns [45]. The regularization during sleep is accomplished by an activity-dependent down-selection system in which synapses that align well with the overall memory organization or have been repeatedly strengthened will survive, whereas others will be depressed [46].

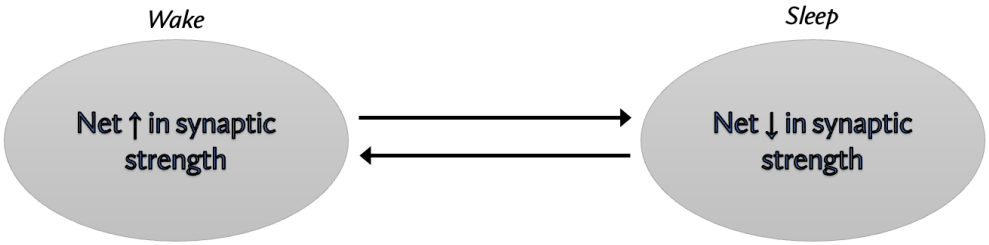

Figure 2.4: The homeostasis hypothesis by Tononi and Cirelli

Several studies have explored different aspects of sleep homeostasis, including molecular and electrophysiological characteristics. The following paragraphs will review the results of some of these studies.

The molecular studies are centred on trafficking of GluA1-containing AMPARs which is a dynamic process involving the movement of these receptor proteins within neurons. The trafficking process allows for the insertion and removal of GluA1-containing AMPARs from the synapse, leading to the enhancement and weakening of synaptic strength, respectively. A rat study reported roughly 40% higher levels of GluA1-containing AMPARs after wakefulness compared with after sleep [47]. Similar GluA1-containing AMPARs' trafficking patterns have been observed in other studies demonstrating the insertion of these receptors during wake and their removal during sleep [48]–[50].

A few studies with electrophysiological approaches employed the slope of the early response evoked by electrical or magnetic stimulation as a quantitative parameter to assess the strength of the synaptic connection between neurons. In humans, an increase was observed in the slope after 18 hours of wakefulness, returning to baseline after an overnight sleep [51]. In-vivo studies on rats have reported similar effects [47], [52]. Consistently, EEG data confirmed a systematic rise in rats' neuronal firing during wakefulness which was regulated during sleep [53]. Similarly, an EEG-MRS study on healthy adults discovered a drop in glutamate levels of the parietal lobe, positively correlated with slow wave activity of EEG [54]. Moreover, a gradual increase in extracellular glutamate levels of rats' cerebral cortex during wake was followed by a decline in the non-rapid eye movement phase of sleep [55].

All the mentioned studies are done in the absence of a learning paradigm. Until now, only a limited number of human studies have investigated the characterization of the sleep-wake cycle under conditions involving learning.

2.3.2 Memory consolidation

Memory consolidation refers to a complex process by which a newly acquired skill will become stable for long-term storage. The consolidation process can take place at the cellular level and system level. Throughout waking hours, especially during active learning, the brain encodes information, forming initial memory traces through synaptic plasticity. Cellular-level consolidation, which initiates immediately after training, stabilizes the encoded memory traces for a short period, typically lasting a few hours. Cellular-level consolidation supports short-term memory. However, for a more durable memory, an additional consolidation stage is needed to transfer information from short-term memory to long-term memory [56]. This addition stage is known as system-level consolidation where memory traces are reorganized and strengthened on a system level. This level of consolidation has been shown to occur during sleep and even rest periods where the cognitive and attentional demand is reduced (offline state).

During these periods, the learning-specific neural patterns are reactivated and eventually transfer the encoded information from fast-encoding temporary storage to long-term storage, leading to the consolidation of memory traces [57]–[59].

Sleep is composed of different stages, including rapid eye movement (REM) and non-rapid eye movement (NREM). Sleep stages are known to play complementary roles in memory

consolidation. Spindles, neuronal oscillation at ~10-15 Hz, are observed during slow wave sleep (SWS) and stage 2 of NREM sleep. Spindles (more importantly high density and clustered spindles) are closely linked to memory reactivation and are therefore known to support system consolidation [60], [61]. On the other hand, the REM stage may stabilize the transformed memory through synaptic consolidation. It is hypothesized that during NREM sleep, the replay of the learning-associated neuronal activity selectively tags the connections that should be further stabilized in REM sleep [62]. There is a growing body of evidence supporting active system consolidation during sleep in rats and humans [63]–[67]. This phenomenon may seem in contrast to the previously mentioned down-selection process centred on synaptic depression, in which the fittest representation among preexisting memory traces will be selected. However, a comprehensive review of the current literature suggests that system consolidation is a process embedded in the global homeostasis of the brain [68]–[70]. This theory suggests that some synaptic connections will be sustained or potentially enhanced while some other synapses responsible for the initial encoding of the experience will be pruned, especially during REM sleep. Structural imaging studies validate the simultaneous occurrence of upscaling within the net downscaling [44], [71], [72]. It is worth mentioning that some studies have shown that the reactivation of memory traces can make previously consolidated memories labile again [73], [74]. Accordingly, the skill acquisition process is depicted in Figure 2.5.

2.4 Neural oscillation

The plasticity and integration of neural circuit components involved in learning is largely dependent on the synchronization of neuronal firing at certain frequencies [75], [76]. Motor learning can modulate neural oscillation in the brain. These changes in neural oscillations can be assessed by electroencephalogram (EEG) capturing the electrical activity of the brain. EEG is characterized by different oscillation frequency bands, including delta (0.1-4 Hz), theta (4-7 Hz), alpha (8-12 Hz), beta (12-30 Hz), and gamma (32-100 Hz). It is challenging to assign a cognitive function solely to a specific band. However, present literature has observed certain associations between these bands and different brain functions. The delta band has been related to learning and motivational processes while theta has been known to reflect working memory and strong emotions [70]–[79]. The alpha band has been associated with short-memory retention whereas gamma oscillations have been connected to sensorimotor integration and higher cognitive processes, like attention and memory formation [73]–

[76]. Moreover, alpha and beta frequency range activity has been shown to be modulated by motor learning[83]–[85].

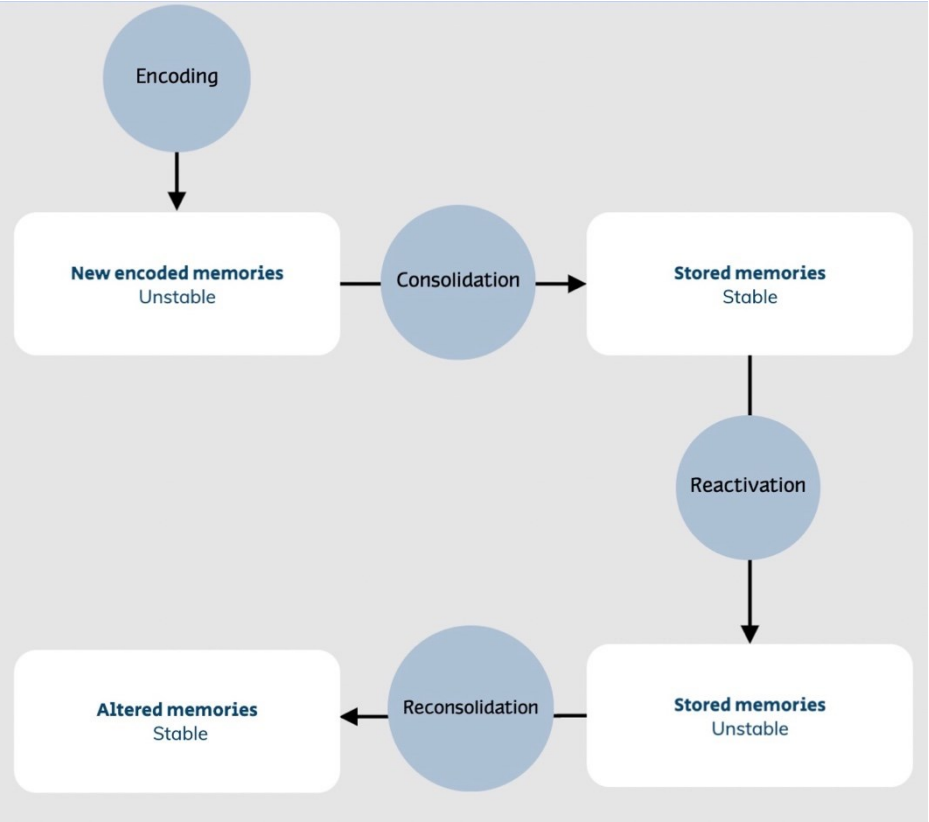

Figure 2.5: Skill acquisition process involving encoding, consolidation, reactivation, and reconsolidation.

An increase in beta oscillations has also been associated with the maintenance of a certain motor or cognitive state [86]. A motor sequence learning study, using a serial reaction time task (SRTT), has found a correlation between performance improvement and beta power suppression [87]. They also reported a decrease in alpha power as learning progressed. Boonstra et al. hypothesize that beta power variation may represent a marker of early consolidation [84]. Additionally, studies have identified a phenomenon known as post-movement beta rebound (PMBR), which occurs following the conclusion of a voluntary movement, particularly in the sensorimotor cortex. This phenomenon is marked by a transient and significant increase in beta frequency synchronization. The characteristics of PMBR can vary depending on factors such as the type of movement task, the complexity of the motor action, and the individual's expertise in the task [81]–[83].

In conclusion, when conducting EEG spectral analysis, it appears reasonable to investigate the activity patterns of all frequency bands, as band-specific modulations could be impacted by the experimental design.

Chapter 3 : Methodology

The previous chapter discussed the existing literature and provided essential insights into the field of study. Following that, this chapter will focus on the methodology of our study offering detailed information about the experimental procedures, data acquisition, and each modality contribution.

3.1 Experimental procedure

To further investigate motor sequence learning, a controlled multi-modal experiment was meticulously designed to assess how learning occurs through inducing variations in glutamate concentration and neural activity. Data acquisition occurred at multiple time points throughout the day to comprehensively capture the entire dynamics of learning. Each participant underwent scanning on two separate days: one motor sequence learning (MSL) day involving a learnable sequence task and one control day with no such sequence involved. The order of sessions was counterbalanced across participants, and each session took place on the same day of the week.

In more detail, the MSL visit lasted approximately thirty hours. Participants arrived around 7 am. They were provided with an overview of the entire day and a consent form to sign. After they changed, they were guided to the PERFORM Centre's physiological suit for the EEG and ECG electrodes to be installed. Electrodes were attached using a medical glue named collodion to ensure they would stay fixed during the entire visit. After installation, we proceeded to the MRI room to start the data acquisition around 9 am. Before the scan, the MRI safety screening form was filled out for each participant by the MRI technician. MRI screening form is a form that primarily assesses whether subjects are claustrophobic, pregnant, or have any metals in their bodies to make sure the strong magnetic field inside the MRI magnet wouldn't be harmful to them and the data will not be affected by artifact.

Each scan lasted roughly one hour, during which an anatomical scan was followed by a simultaneous fMRI-EEG recording and two MRS imaging sessions—one for each region of interest (ROI): the supplementary motor area (SMA) as the motor-implicated region, and the posterior cingulate cortex (PCC) as the control region, which is known to be involved in sleep homeostasis. Participants were

asked to keep their eyes open during the fMRI-EEG recording period to avoid eyes-closed modulation of neuronal oscillations. After the first scan, they learned the motor sequence for the first time. Then, they underwent two other scans, one right after the task at 11 am and another at 1 pm. After the third scan, they were provided with a lunch and had a few hours to rest. Afterwards, they practiced the MSL task again during a recall session right before proceeding to the fourth scan at 5 pm. The last scan of the day, the fifth scan, was done at 9 pm after which they had their dinner and were prepared for an overnight stay in the PERFORM's sleep lab.

Before they sleep, some facial electrodes were added to the previous setup to conduct overnight polysomnography (PSG). PSG is a sleep study where participants' heart rhythm (ECG), eye movements (EOG), and muscle activities (EMG) are monitored along with their brain electrical activity (EEG). The PSG data will be analyzed as a future work of this study to explore different stages of sleep and their corresponding memory processes. The following morning, participants were woken up at 7:30 am. After having their breakfast, they were guided to their last scan, which took place at the same time as the first scan, at 9 am. After the scan, their overnight performance gain was measured through an MSL practice session. Lastly, the electrodes were carefully removed using collodion remover and participants' heads were then cleaned to ensure proper hygiene and comfort.

The control visit occurred on the same day of the week as the MSL visit, with a time gap of 1-3 weeks. The protocol was similar to MSL day, excluding the overnight stay and the subsequent morning acquisition. The primary difference was that the practiced sequence did not involve a learning component and served only as a control for the movements. The study protocol is demonstrated in Figure 3.1

Participants were asked to follow a regular sleep-wake schedule, synchronized with circadian rhythm (11 pm - 7 am ±1h), for at least two weeks before each visit. A week before, they were supposed to limit their alcohol and caffeine consumption and avoid any cannabis intake. Finally, a day before their visit, they were asked to avoid alcohol, coffee, magnesium (complements, chocolate, banana, pitted fruit), and sugary drinks as much as possible to avoid glutamate modulation or sleep-wake cycle distortion.

Before each scan, the participant's saliva sample was collected to measure the average cortisol concentration indicating the participant's stress level. To evaluate the participant's sleep-wake cycle, several saliva samples were taken throughout the day to measure the average melatonin concentration. Moreover, during their rest periods, participants were only allowed to engage in simple entertainment. Stressful activities or studying were prohibited to avoid triggering non-learning-specific neuronal plasticity or cognitive processes.

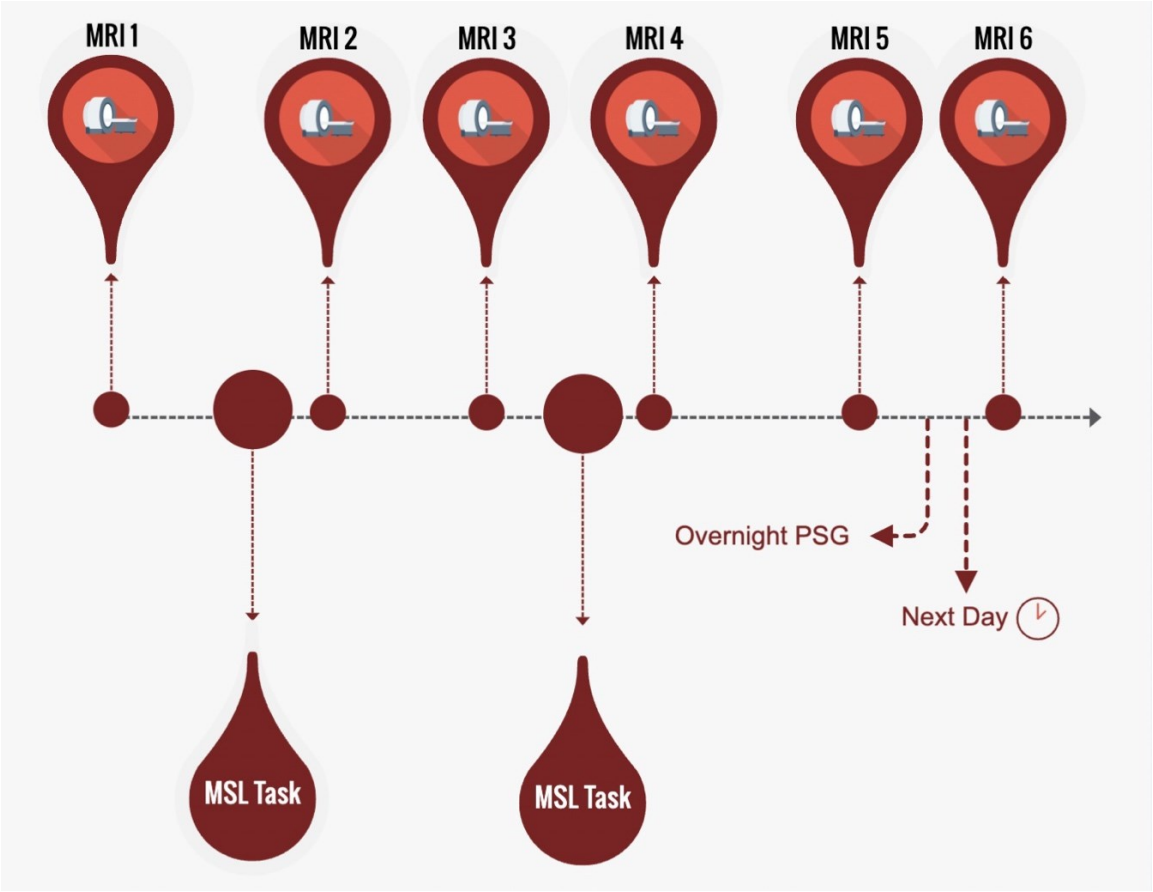

Figure 3.1: Study design including six data collection throughout the waking period, specifically at 9:00, 11:00, 13:00, 17:00, 21:00 and then again at 9:00 on the following day.

3.1.1 Task design

Motor sequence learning was tested using the sequence finger-tapping task employed by Laventure, S. et al. [61], which is a modified version of the paradigm initially developed by Karni, A. et al. [23]. Subjects repeatedly performed a predetermined sequence of eight-element finger

movements with their left (non-dominant) hand as long as a green square was displayed on the screen. The sequence was explicitly introduced to the participants, and they were asked to be as fast and accurate as possible. Practice blocks of the motor sequence were interspersed with 30-second rest periods (Figure 3.2). A response box with four buttons placed in a horizontal row was utilized to record the sequences and measure the reaction time between each key press as well as each sequence performance duration. No performance feedback was given to the participants during the entire visit.

The control task was also composed of an eight-finger pressing sequence that involved no sequence-specific learning to control for the finger movements and their potential neural plasticity triggering.

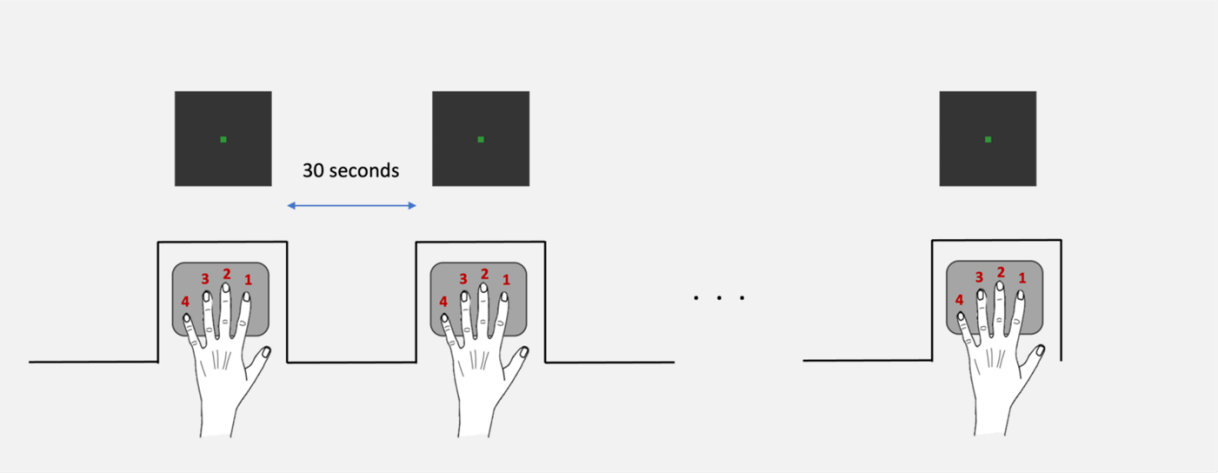

Figure 3.2: Task design

3.1.2 Sample size

The sample size is a crucial factor in addressing any study's hypotheses. It should be large enough to achieve sufficient power in statistical analyses. Our study is a preliminary experiment involving five healthy male participants. The statistical analyses were adjusted to balance the number of participants as much as possible while ensuring adequate representation for meaningful results.

3.1.3 Inclusion criteria

Participants were selected from healthy young adults aged 18 to 35. They were right-handed individuals with good sleeping cycles. Highly skilled typists, gamers, or musicians were excluded due to their previous professional training in motor sequences which could impact the intended learning process.

Participants' sleeping patterns and diet were evaluated due to their influence on the circadian rhythm and the brain's chemical state. To do so, we employed the insomnia severity index and the Epworth sleepiness scale self-report questionnaires. The insomnia severity index (ISI) is designed to assess the severity of insomnia. It comprises seven questions covering various aspects of insomnia, including difficulties with sleep onset, sleep maintenance, early morning awakening, satisfaction with sleep, interference with daily functioning, noticeability of impairment attributed to sleep problems, and distress caused by sleep difficulties. Respondents rate each item on a Likert scale, allowing for a quantitative evaluation of insomnia severity. The Epworth sleepiness scale (ESS) is designed to measure daytime sleepiness and assess the likelihood of falling asleep in various situations that demand alertness. Comprising eight items, the ESS prompts respondents to rate their likelihood of dozing off or falling asleep on a scale ranging from 0 to 3, with higher scores indicating greater daytime sleepiness. The scenarios presented in the questionnaire cover a spectrum of daily activities, from sitting and reading to watching television or attending a meeting. The ESS provides a quantitative measure of subjective daytime sleepiness which could help to ensure participants will probably not fall asleep during their rest periods or while they are inside the MRI scanner.

3.2 Data acquisition

As previously mentioned, this study aims to evaluate the variation in glutamate concentration and neural activity resulting from motor learning. Quantifying these changes is achievable by using Magnetic Resonance Spectroscopy (MRS) and Electroencephalogram (EEG), respectively. MRS and EEG imaging techniques will be introduced in the following sub-chapters while providing further details on their configuration in this specific study.

3.2.1 Magnetic Resonance Spectroscopy (MRS)

Magnetic resonance spectroscopy (MRS) is a non-invasive imaging technique that allows us to measure the concentration of different biochemicals in the brain. MRS relies on the same principles as a commonly known technique called magnetic resonance imaging (MRI) and can be acquired by adding predetermined sequences to an MRI scanner (Figure 3.3). MRI generates anatomical images of the brain using the signal from water protons whereas MRS generates a spectrum from a small localized region of interest using the signal from protons in different chemicals [91]. It detects signals from proton nuclear spins by subjecting a sample to a strong external magnetic field and applying a radiofrequency (RF) pulse to this field. The RF pulse temporarily disturbs the alignment of nuclear spins, leading to signal emission as the spins return to their original alignment. The emitted signals, detected as RF waves, undergo frequency analysis to produce a spectrum. Different chemical environments and nuclei in the sample resonate at distinct frequencies, allowing for the identification and quantification of specific compounds [92]. Therefore, MRS is a powerful method for analyzing the chemical composition of a tissue which can be used to study various diseases such as cancer [93]. Epilepsy [94], Alzheimer's disease [95], and Parkinson's disease [96].

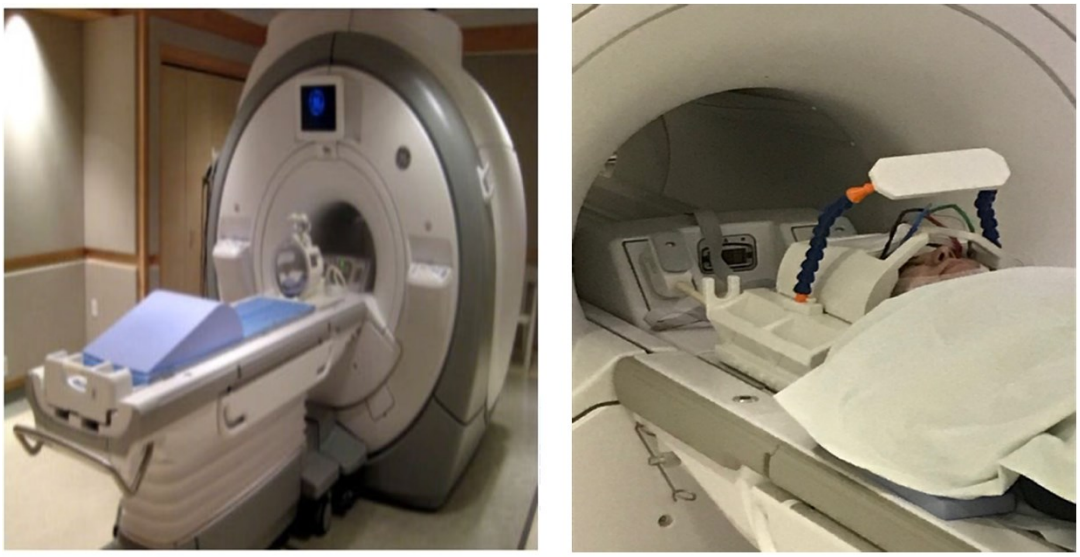

Figure 3.3: a) The MRI scanner at Perform Centre. b) Our setup inside the scanner.

An MR spectrum is formed from the frequency distribution of several different metabolites, including Glutamate (GLU), Lactate (Lac), Total Creatine (tCr), Myo-inositol (Ins), Glyceryl phosphorylcholine (GPC), Total N-acetyl aspartic acid (TNAA), and Macromolecules (MMs). These metabolites contribute to different peaks in the spectrum which are expressed in parts per million (ppm) (Figure 3.4).

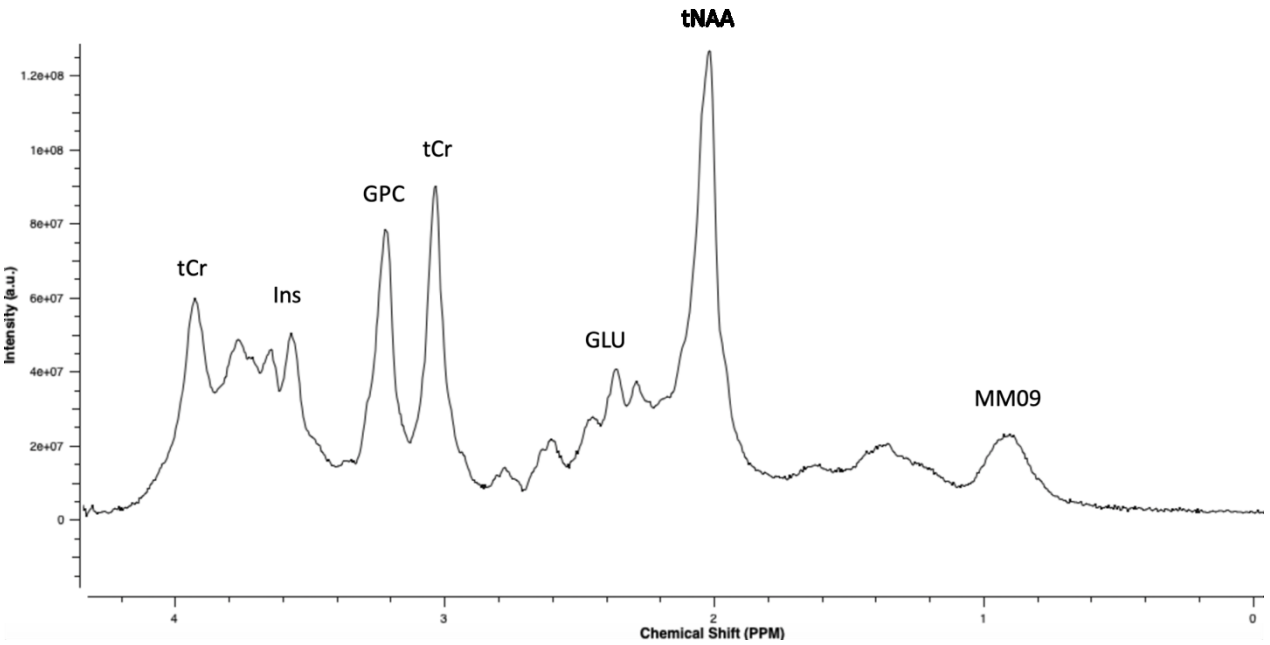

Figure 3.4: An MR spectrum showing peaks for Glutamate (GLU), Total Creatine (tCr), Myo-inositol (Ins), Glyceryl phosphorylcholine (GPC), Total N-acetyl aspartic acid, and Macromolecules at 0.9 ppm (MM09).

While MRS is indeed a valuable tool for quantifying a wide range of metabolites, it does require expertise in determining the scanner sequence parameters to effectively target the desired metabolite. Using a 3T GE MRI scanner, we implemented a Point Resolved Spectroscopy (PRESS) sequence with the following sequence parameters: TR = 2000, TE = 35ms, 152 averages, 4096 spectral points, 4500 Hz spectral width, and 8-step phase cycling. The long echo time of 35 milliseconds was chosen to enable the detection of glutamate while suppressing the overlapping macromolecules due to T2 relaxation. To be able to detect and quantify the metabolites accurately, it is necessary to minimize the interference caused by water molecules as they will produce a much stronger signal. To address this issue, we implemented CHESS (Chemical Shift Selective) water

suppression, a technique commonly used in MRS acquisition to selectively suppress the signal from water molecules using the resonant frequency of water protons.

As glutamate shares the same molecular structure with an amino acid named glutamine, its MR spectra will overlap and get contaminated with glutamine's spectra. In this study, MRS acquisition parameters were optimized to enhance the differentiation of glutamate and glutamine, aiming to assess glutamate concentration solely. The PRESS sequence was employed with TE of 35 ms — as shown in previous studies, the optimal TE for differentiating glutamate and glutamine spectra obtained by PRESS is between 30-40 ms [97]. To further assist the separation, the spectra were collected in high spectral resolution using 4096 spectral points. After processing the spectra, low cramer-rao lower bounds (CRLB), a common measure indicating the uncertainty of the estimated parameters, verified the optimal separation of these biochemicals.

As mentioned earlier, MRS is most widely performed as a single-voxel spectroscopy (SVS) technique where the sequence is applied to a compact region of interest (ROI). This method is able to provide high signal-to-noise (SNR) in a relatively short scan time making it suitable for quantitative analysis. In our study, we targeted two large ROIs (voxel size of 4 cm x 4 cm x 3 cm = 48 cc): supplementary motor area (SMA) and posterior cingulate cortex (PCC). In the following subchapters, we will provide a brief overview of each region and explain why they were selected.

Supplementary Motor Area (SMA)

Supplementary Motor Area (SMA) is located in the dorso-medial surface of the frontal cortex, in the superior frontal gyrus [5] (**Error! Reference source not found.**). SMA plays a crucial role in the preparation and execution of voluntary movements [20]. Therefore, SMA will be involved in motor sequence learning through its role in motor planning and coordination. Moreover, motor sequence learning is closely associated with procedural memory, which is the memory for skills and habits. The SMA contributes to the formation and consolidation of procedural memories related to motor sequences [17]. Changes in SMA have been observed during the progress from the early stages of learning to the more proficient execution of a motor sequence [5], [20]. Accordingly, SMA would be a suitable region to track during different stages of motor sequence learning.

Posterior Cingulate Cortex Area (PCC)

The Posterior Cingulate Cortex (PCC) is in the medial region of the inferior parietal lobe, in the posteromedial cortex, right above the corpus callosum (Figure 3.5**Error! Reference source not found.**). PCC is an essential part of the default mode network (DMN), implicated in various cognitive functions, including attention, self-referential processing, mind-wandering, and some aspects of memory [98], [99]. PCC also plays a role in consciousness regulation and sleep homeostasis during which memory consolidation takes place [100]. Furthermore, PCC has no explicit association with motor learning making it an ideal candidate for the control region.

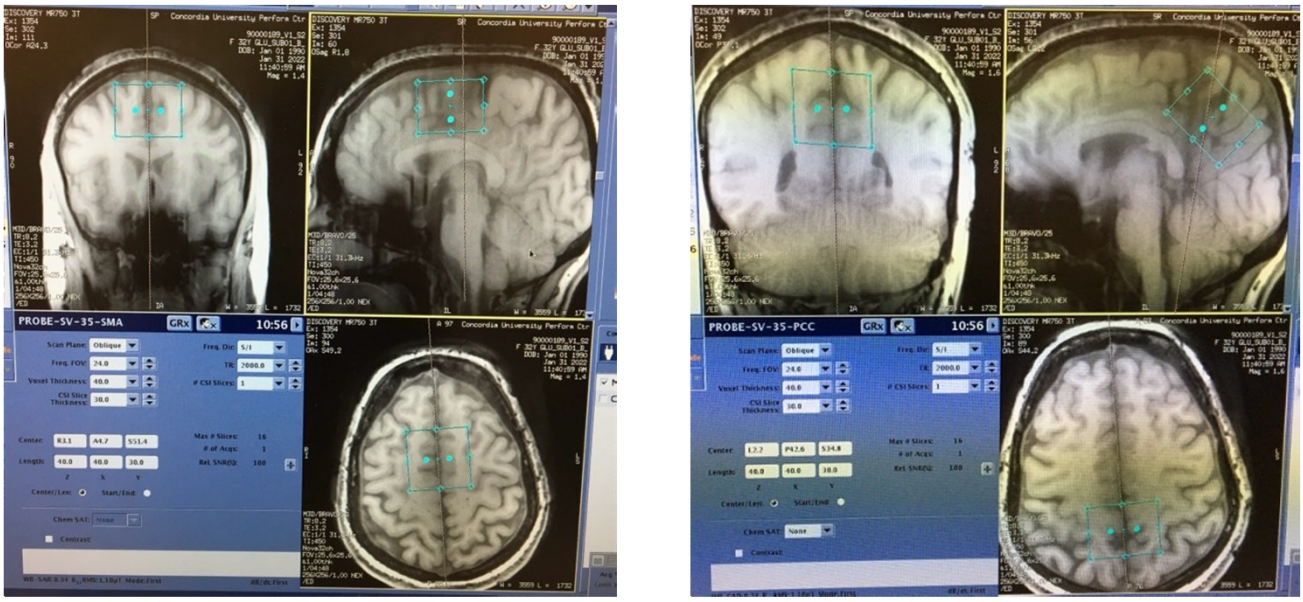

Figure 3.5: Regions of interest: a) Supplementary motor area (SMA). b) Posterior cingulate cortex (PCC).

3.2.2 Electroencephalogram (EEG):

Electroencephalogram (EEG) is a non-invasive test that captures the brain's neuronal activity by measuring the electric potential difference across different areas of the scalp. This voltage variation is produced by cortical pyramidal neurons perpendicular to the brain's surface. When large local groups of neurons fire, they generate excitatory and inhibitory postsynaptic potentials summing into a field potential which is detectable by EEG. Contrary to common belief, EEG is

not generated by action potentials as they have a much shorter duration and their amplitude decay rapidly as they travel through axons [101]. EEG is able to record real-time electrical activity of the brain with a great temporal resolution. Therefore, like MRS, EEG has various applications in both research studies and clinical diagnosis. EEG can be employed to diagnose neurological disorders, such as Alzheimer's disease [102], epilepsy [103], or sleep disorders [104], In the research domain, EEG serves as a fundamental tool for investigating the brain including its responses to stimuli, cognitive processes [105], and connectivity [106]. An EEG recording is composed of several waveforms recorded by different channels (electrodes) of an EEG device (Figure 3.6).

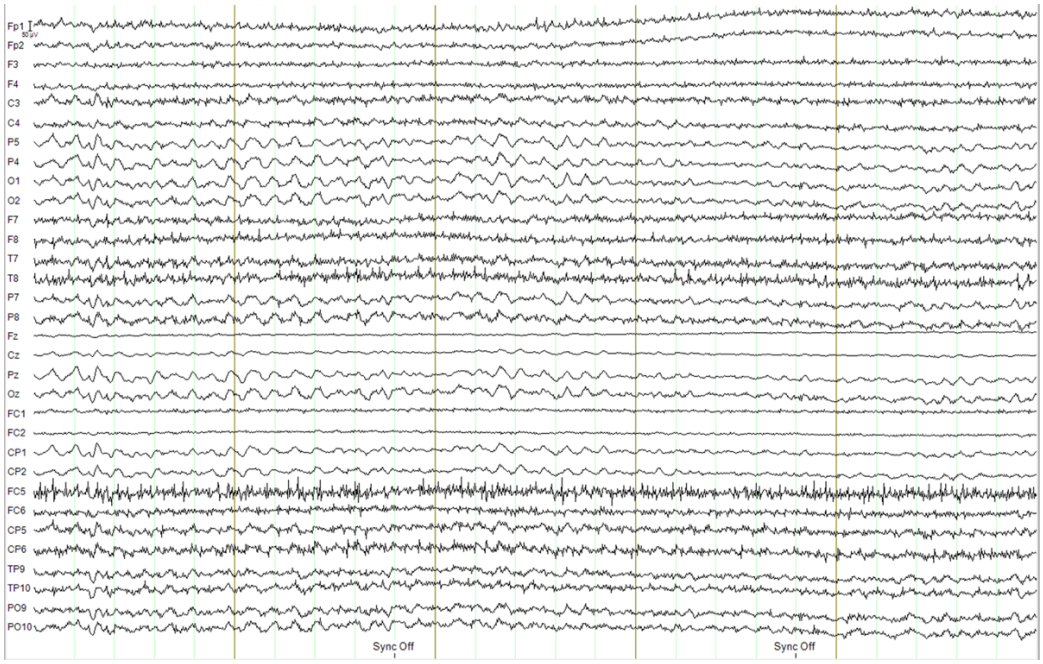

Figure 3.6: An EEG signal showing waveforms of 32 channels.

In this study, we utilized a 32-channel EEG device custom-designed with free electrodes based on our protocol and the setup at the PERFORM Centre. After taking each participant's head measurements, anatomical landmarks were specified, the location of each electrode was marked, and electrodes were installed following the 10-20 system, a standardized method for electrode placement which is named for the distances between adjacent electrodes being either 10% or 20% of the total anteroposterior and lateral distance on the scalp (Figure 3.7). Before installing the

electrodes, alcohol pads and skin prep gel were used on the predetermined location to reduce the scalp impedance and ensure better signal quality. To avoid electrode movement during visits, electrodes were glued to the scalp using collodion. The EEG setup is shown in Figure 3.8.

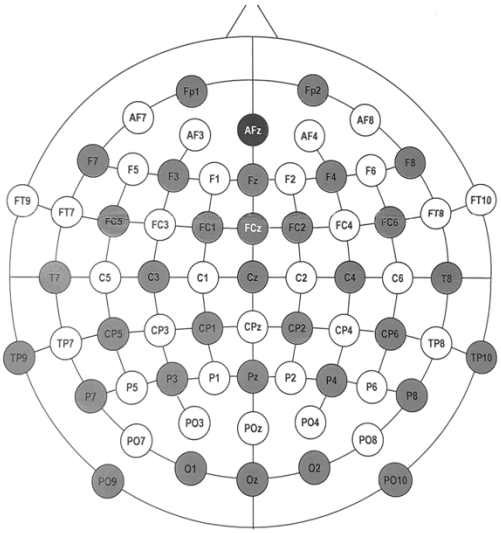

Figure 3.7: The 10-20 system employed for electrode placement, utilizing only the 32 darker channels, with AFz and FCz serving as the ground and reference, respectively.

Figure 3.8: EEG setup

ECG electrodes were installed on the left side of the participant's back forming a dipole crossing

the heart. Optimal locations were determined by several pilot studies. The skin was prepared before the installation, as reducing the impedance is crucial for detecting the ECG signal.

Using the Brain Products software, EEG data was recorded inside the MRI scanner and transferred to the laptop with fibre-optic cables, and the hardware was synchronized to the master clock of the scanner using a sync box. The fMRI-EEG setup is illustrated in Figure 3.9.
EEG sampling rate and resolution were set at 5000 Hz and 0.5 μV respectively. Recordings were referenced to FCz and filtered with a 10 s time constant low cut-off filter and a 250 Hz high cut-off filter to prevent DC saturation and limit the gradient artifact. Bipolar ECG recording was done with a resolution of 10 μV as it is more susceptible to saturation.

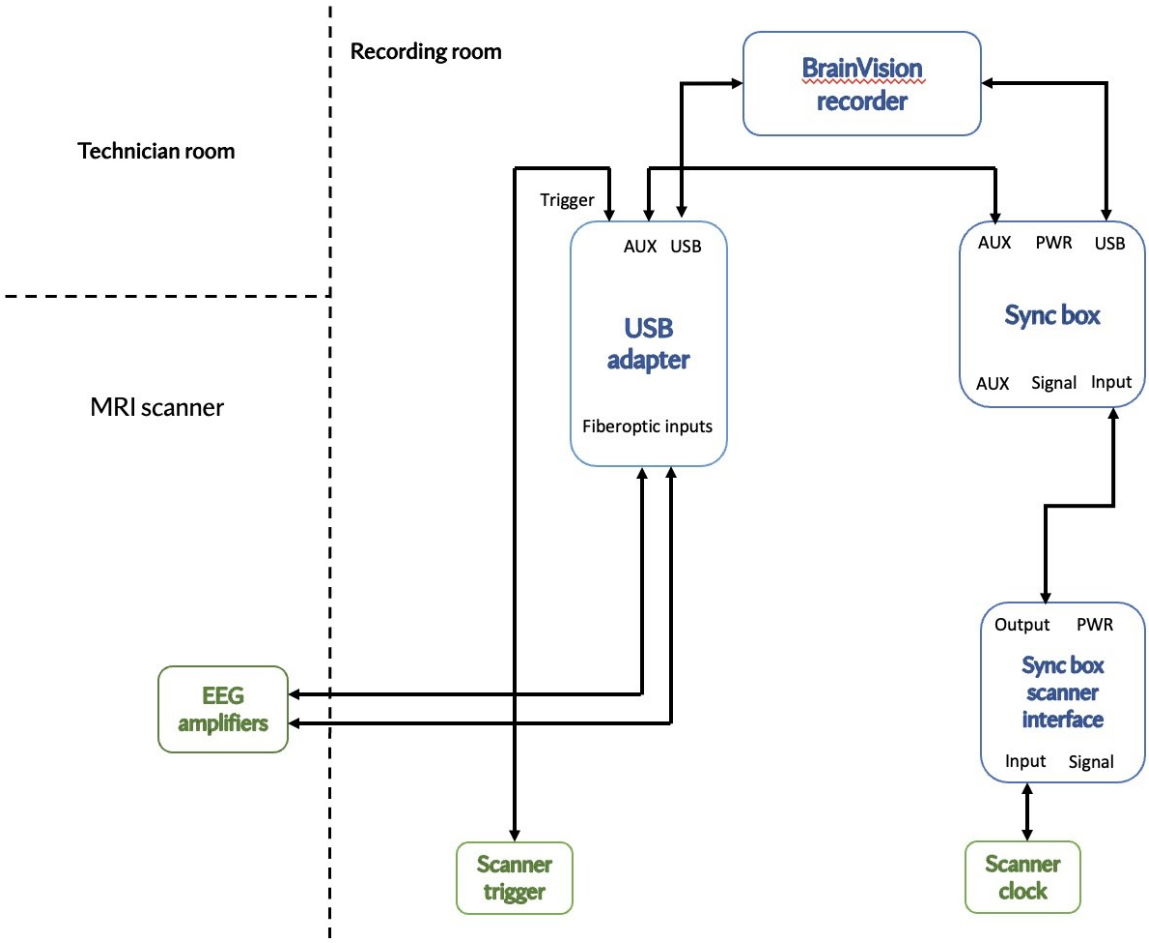

Figure 3.9: EEG-fMRI configuration

3.2.3 Functional magnetic resonance imaging (fMRI):

Functional Magnetic Resonance Imaging (fMRI) is a non-invasive neuroimaging technique that captures dynamic changes in blood flow to infer neural activity within the brain. Operating on the principle of neurovascular coupling, fMRI relies on the fact that increased neuronal activity in a specific brain region will raise the demand for oxygen and nutrients which will lead to heightened local blood flow. The fMRI machine detects the blood oxygen level-dependent (BOLD) changes, particularly variations in the magnetic properties of hemoglobin caused by changes in the ratio between oxygenated hemoglobin (oxyhemoglobin) and deoxygenated hemoglobin (deoxyhemoglobin) [107]. By detecting these changes, fMRI provides insight into the functional organization of the brain which is useful in studying cognitive processes, mental health, pre-surgical planning, and various neurological disorders [108].

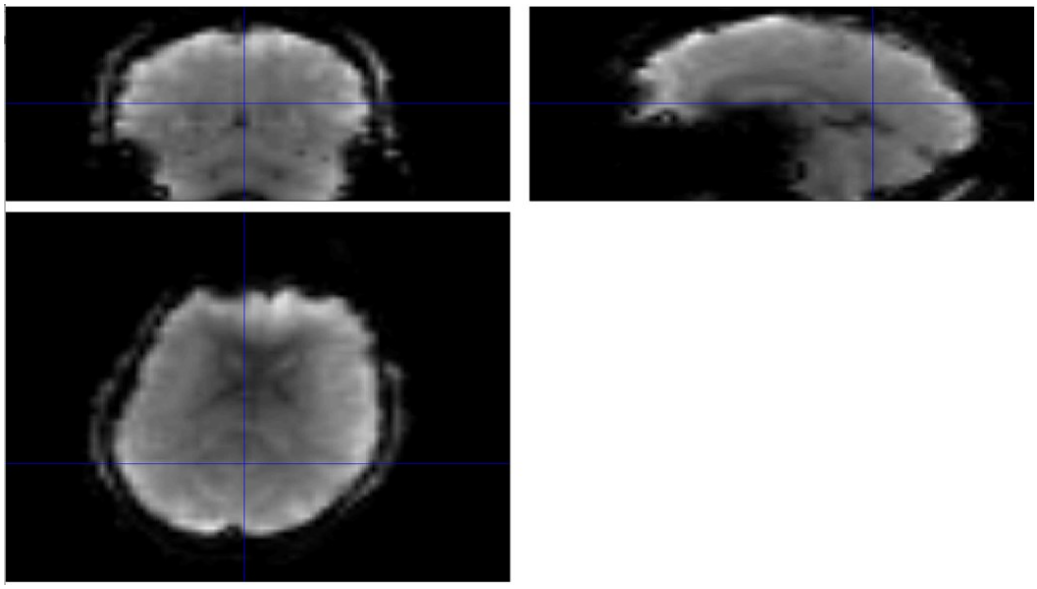

Figure 3.10: A raw fMRI sample

In this experiment, functional MR images, as illustrated in Figure 3.10, were collected using repeated single-shot echo-planar imaging with the following characteristics: TE = 30 ms, FA = 90°, in-plane resolution = 2 x 2 mm2, 75 slices acquired in an ascending and interleaved order, slice thickness = 2 mm and TR = 1700 ms. Also, a field map acquired using a double echo gradient echo sequence was used to correct for geometric distortions due to magnetic field non-homogeneities.

Chapter 4 : Data analysis

Following the data collection methods covered in the previous chapter, this chapter will discuss the data format, preprocessing and processing approach for each modality as well as the employed software, along with the postprocessing statistical analysis.

3.1 MRS data analysis

Each MRI scanner produces raw data in a distinct format which requires preprocessing and processing to quantify the concentration of each metabolite. A GE scanner generates Pfiles (.7) including the raw k-space data, the data collected in the frequency domain before conversion to the spatial domain, as well as some acquisition parameters which are placed in the header. In the upcoming section, we will introduce the common procedures involved in preprocessing the raw MRS data.

3.1.1 Preprocessing

Each raw data file typically contains two data types: unsuppressed water reference data, and water-suppressed data obtained during water suppression sequences such as CHESS. The unsuppressed water data serves as a reference for the water signal and is useful for making corrections and doing normalization in some preprocessing steps. This section will cover the main preprocessing steps of MRS data.

1. Coil combination:

As MRI scanners are usually composed of several Radio Frequency (RF) coil receivers, the first preprocessing step would be to combine the data collected from different coils. Since the coils' locations with respect to the voxel of interest are different, each coil receiver collects the signal with a different phase and signal-to-noise ratio (SNR). Proper complex weights need to be estimated and applied to adjust the amplitude and phase of each coil signal such that it maximizes the SNR and makes the coils' signals phase-coherent [109]. This step is crucial for subsequent analysis.

To calculate the complex weights, the water reference data will be utilized. Since the water signal appears almost the same from each coil, it can be averaged through all the elements to achieve the water reference data with high SNR.

2. Removing motion corrupted averages:

The overall spectra can be inspected by the MRI technician to ensure it has acceptable quality. In addition, the coil combined averages should be rechecked, and all the motion-corrupted averages should be removed as they can create distortion in the next steps.

3. Phase and frequency alignment:

Phase and frequency drifts are common in acquiring MRS data. It can be created due to physiological factors, such as respiratory effects and cardiac pulsation, creating small movements. It can also occur because of the small variation in the scanner magnetic field which can result from temperature changes of scanner components.

There are different types of algorithms for correcting the abovementioned drift. Some algorithms use individually acquired navigator echoes or require non-water-suppressed acquisition techniques which are not applicable to most clinical MRS acquisitions including the one in our study. Some other methods try to track either the residual water or creatine peak making them dependent on the existence of a metabolite peak with an acceptable SNR. To perform well, these methods need to be adjusted based on each MRS acquisition. On the other hand, there are more recently developed algorithms that use the full spectrum to estimate and correct the drift. One of these methods is spectral registration which temporally aligns the spectral averages to a chosen reference [110], [111]. In this experiment, we will use spectral registration to correct for phase and frequency drifts in MRS data as they can broaden the peaks and distort the spectrum affecting the accuracy.

4. Combining averages:

Now that all the averages are coil combined and aligned, we can combine all the averages to compose one unified spectrum with higher SNR. It is recommended to use the arithmetic mean to combine the averages.

5. Eddy's current correction:

Eddy currents refer to transient currents induced in conducting components of the scanner by the rapid changes in the magnetic field associated with gradient pulses [112]. They can create time dependency in the frequency domain leading to distortions in the spectrum. Since this effect will appear as a deviation from linearity in the phase function of the water signal, the water reference

data can be used to compensate for it [113].

6. Residual water peak removal:

As previously mentioned, we use a CHESS water suppression technique to minimize the water signal. However, even by applying the suppression method, some water residual peaks will still arise in the acquired spectrum. The residual water peak can be detected and removed by employing singular value decomposition techniques such as HLSVD [114].

7. Phase correction:

To prevent spectral broadening, it is common to only present the real part of the acquired complex signal in an MR spectrum making the spectrum appearance susceptible to the phase of each point. Phase correction involves adding either a constant or a linear phase shift to the spectrum until it becomes in-phase. The aim is to convert the spectrum to a purely positive absorptive mode meaning all the main singlet peaks would be positive and symmetric with no zero-crossing [115].

3.1.2 Fitting

After the raw spectrum is preprocessed, the fitting will be performed to assess each metabolite concentration. The most common fitting method uses a linear combination model. In this method, each metabolite contribution is modelled as a single spectrum showing its response function according to the employed MR sequence. From these single spectra, a basis spectra set will be built, containing different metabolites' spectral contributions. The amplitude, frequency, phase and linewidth of these basis spectra will be adjusted, and their linear combination will be fitted to the obtained MR spectrum through a nonlinear least-squares approach. The estimated amplitudes will represent the signal intensity of the metabolites, and the residual unexplained data can indicate the quality of the fit [115].

To improve the fit, it is recommended to account for macromolecule contribution in the basis set. Macromolecules (MMs) are larger molecules such as proteins and lipids with broad spectrum characterizations that can distort the baseline and mask the weaker signals. A simple way to include them in the basis set is by using parameterized models for the well-known MMs, including MM09, MM12, MM14, MM17, and MM21.

3.1.3 Quantification

To obtain metabolite concentrations in conventional units, such as mM, it is necessary to relate the fitted signal intensity to another chemical concentration. The commonly employed reference is the unsuppressed water data, which represents the water signal within the tissue. This choice is motivated by the fact that this signal is acquired under identical conditions from the same region of interest using the same sequence, has a significantly stronger signal, and is less susceptible to overlapping with other signals [115].

3.2 MRS software

For preprocessing and fitting of the obtained MR spectrum, two approaches were taken. In the first method, the FID-A toolbox was used for preprocessing the raw spectra and Tarquin was employed for fitting the processed spectra and assessing glutamate concentrations. The second method was more user-interactive. The basis set was simulated using an MRSCloud, and the acquired spectra were preprocessed and fitted through a pipeline created in FSL-MRS. The mentioned software and comprehensive information on each method will be discussed in the following part.

3.2.1 FID-A

FID Appliance (FID-A) (*www.github.com/CICmethods/FID-A*) is a free, open-source, MATLAB-based software. This package is composed of different toolboxes that can be utilized for the design and analysis of RF pulses, MRS simulation, and processing of MRS data. In our first approach, FID-A handled the preprocessing of the raw MRS data. FID-A provides a fully automated preprocessing pipeline specifically designed for different scanner vendors and MR sequences. The script for GE PRESS MRS data accepts GE raw data in Pfile format, and it primarily involves coil combination, removal of corrupted averages, and frequency alignment. As a result, the toolbox will distinctly output the preprocessed water-suppressed and water-unsuppressed data files with the LCModel RAW format [116].

3.2.2 Tarquin

Tarquin (www://tarquin.sourceforge.net) is a free, open-source analysis tool used to

quantify different metabolites' concentrations in MRS data. Tarquin provides the opportunity to carry out the data analysis using both GUI and command-line environments. The command line version facilitates batch processing whereas the GUI version allows a more user-interactive data analysis.

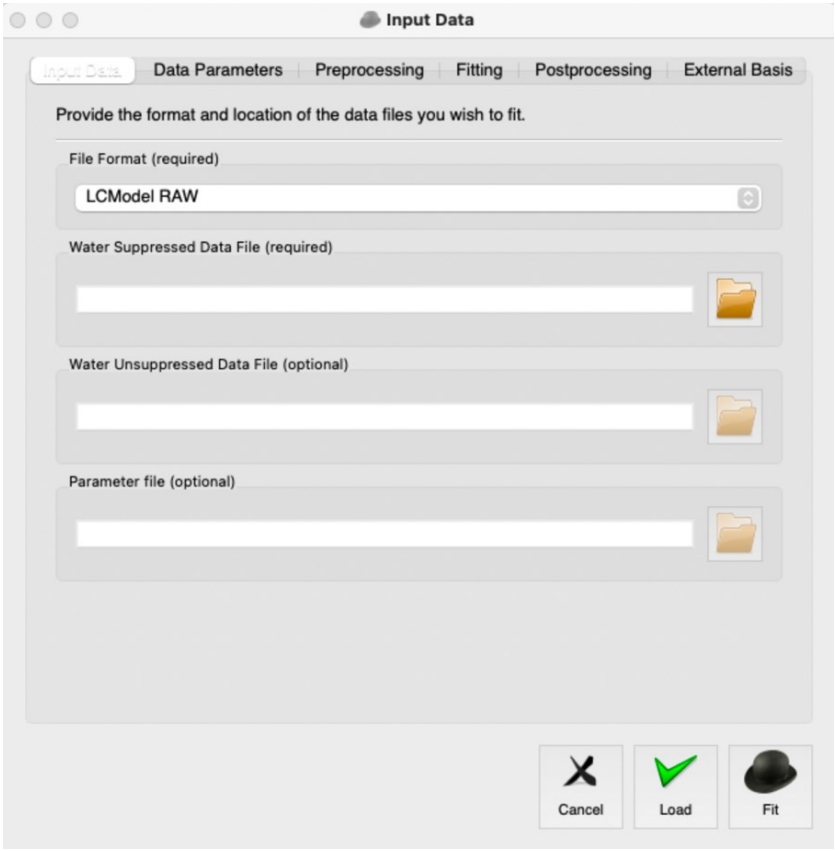

Figure 4.1: Tarquin GUI interface

As shown in Figure 4.1, the software accepts versatile file formats and allows for different parameter adjustments related to data acquisition and processing. For this experiment, the preprocessed data provided by FID-A was used as the inputs and the parameters were set according to Table 1. The fit quality was controlled through the GUI interface, but the data processing was performed using the command line version. A sample fit can be observed in Figure 4.2.

Table 1: Tarquin's input parameters

	Tarquin's parameters
Input data	*File Format: LCModel RAW* *Input Data Files: Water Suppressed Data and Water Unsuppressed Data*
Data parameters	*Sampling frequency (Hz): 5000* *Transmitter frequency (Hz): 127.764294E6* *Echo time (s): 0.035* *Data points: 4096*
Preprocessing parameters	*Water cutoof (Hz): 45* *Reference offset (ppm): 4.65* *Eddy current correction*
Fitting parameters	*Start point: 5* *End point: 2048* *Maximum iteration: 75*

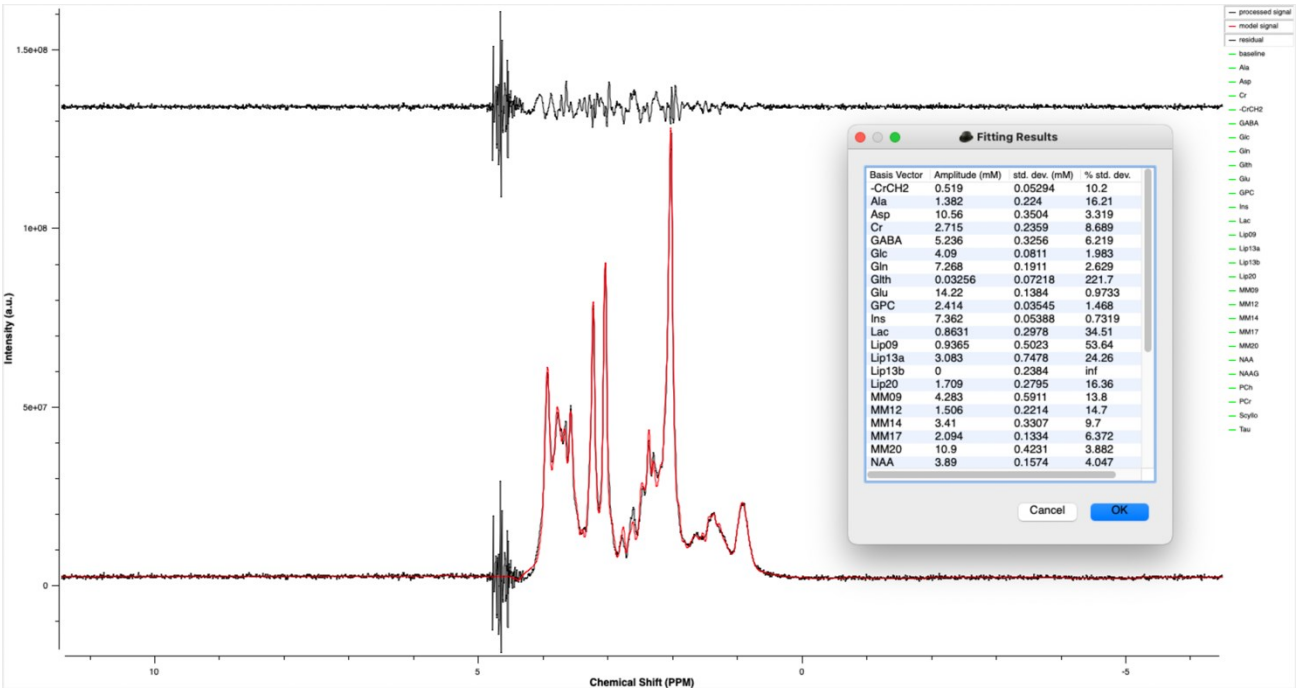

Figure 4.2: Tarquin's sample fit

3.2.3 FSL-MRS

FSL-MRS is an open-source, python-based software that can be used for MRS data conversion, preprocessing, basis spectra simulation, and fitting and quantification.

Analysis can be scripted and run via the command line for batch processing. For a more interactive way, Python notebooks may be used [117].

Unlike Tarquin, this software only accepts input data with a NIfTI format. Therefore, the package is paired with a conversion tool named spec2nii which can convert different MRS data formats to NIfTI. We have created a preprocessing pipeline in FSL-MRS including data conversion, coil combination, phase and frequency alignment, averaging, eddy current correction, water residual removal, and phase correction. Then, the basis spectra set needs to be simulated, as FSL-MRS cannot create it automatically by using the information from MRS data. FSL-MRS offers a command line interface for the simulation of the basis spectra. However, it needs the full description of one sequence repetition in a JSON file. The GE scanner utilized in this experiment was not able to provide all the sequence parameters. Therefore, we used a cloud-based tool named MRSCloud to simulate a basis set according to our sequence [118]. Using the basis set, the spectrum was fitted by FSL-MRS to quantify glutamate concentration (Figure 4.3).

Metab	unscaled	CRLB	%CRLB	/Cr+PCr
Ala	0.03	0.012	42.9	0.12
Asc	0.07	0.007	10.2	0.3
Asp	0.13	0.019	14.4	0.55
Cr	0.24	0.012	5	1
CrCH2	0.09	0.007	7.2	0.39
EA	0	0.01	999	0
GABA	0	0.014	999	0
GPC	0.06	0.004	6.8	0.27
GSH	0.04	0.004	8.8	0.19
Gln	0	0.015	999	0.01
Glu	0.35	0.012	3.6	1.46
Gly	0.09	0.007	8.1	0.37
H2O	0	0.242	999	0
Lac	0	0.016	999	0
MM09	0.14	0.007	4.8	0.58
MM12	0.04	0.016	40.4	0.17
MM14	0.06	0.019	29.9	0.27
MM17	0.12	0.021	16.9	0.53
MM21	0.02	0.012	69.2	0.07
NAA	0.27	0.006	2.2	1.13
NAAG	0.07	0.004	6	0.3
PCh	0	0.005	999	0
PCr	0	0.011	999	0
PE	0	0.014	999	0
Ser	0.04	0.009	22.7	0.17
Tau	0.03	0.005	17.7	0.12
mI	0.11	0.009	8.7	0.46
sI	0	0.001	38.5	0.01
Cr+PCr	0.24	0.004	1.5	1

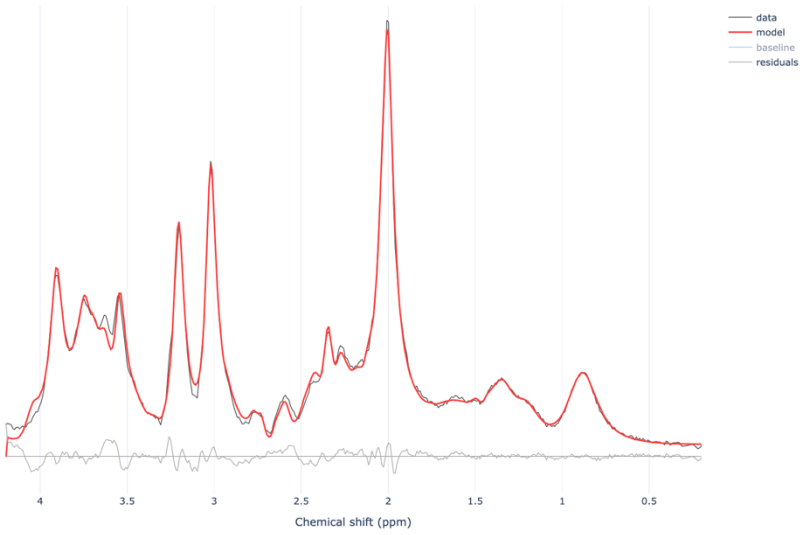

Figure 4.3: FSL MRS sample fit

3.3 EEG data analysis

The EEG signal was recorded using BrainVision recorder which stores the data in three files: the header file (.vhdr) containing a description of EEG, the marker file (.vmrk) listing the events and their properties, and the actual data file (.eeg) with the voltage values. EEG data recorded inside an

MRI scanner will be heavily contaminated by different types of artifacts. Hence, preprocessing steps should be taken to minimize the noise effect on further analysis. This section will present different artifact types, preprocessing steps to tackle them, postprocessing analysis, and utilized software for each part.

3.3.1 Preprocessing

The main artifacts affecting the EEG data simultaneously acquired with fMRI are gradient artifacts and ballistocardiogram artifacts [119].

1. Gradient artifact (GRA):

Constant switching of gradients during fMRI acquisition will repeatedly change the magnetic field inside the scanner. According to Faraday's law, changes in magnetic field will cause electromagnetic induction in electrodes and cables creating a huge broad-band artifact on EEG with much greater amplitude than the EEG signal.

2. Ballistocardiogram (BCG) / pulse artifact:

The BCG artifact originates from the electrodes' movement resulting from cardiac-driven motion, especially the pulse under the scalp.

Other artifacts, such as motion artifacts and environmental artifacts, may also affect the EEG signal but their impact is not as significant as the abovementioned artifacts. However, these are harder to identify and remove because of their non-repetitive structure. To minimize the environmental artifacts, the scanner's helium cooling pump was turned off during the EEG-fMRI acquisition.

The preprocessing steps were carried out using BrainVision Analyzer (actiCHamp Plus, Brain Products GmbH, Gilching, Germany). Data was bandpass filtered from 0.5-55 Hz. To correct for gradient and pulse artifacts, average artifact subtraction (AAS) was employed taking advantage of the artifacts' repetitive structure (Figure 4.4). In this method, the average of different artifact intervals will be used as an artifact template for the original interval of interest. Then, the template will be subtracted from the relevant interval to minimize the artifact effect [120].

For gradient artifact correction, instead of selecting different intervals for template calculation, we opt for sliding average over a fixed number of time repetitions. The sliding average will accommodate minor fluctuations in the artifact, possibly arising from slight head movements, while producing a more stable template. Moreover, a semiautomatic R-peak detection approach

was pursued to calculate the pulse artifact average.

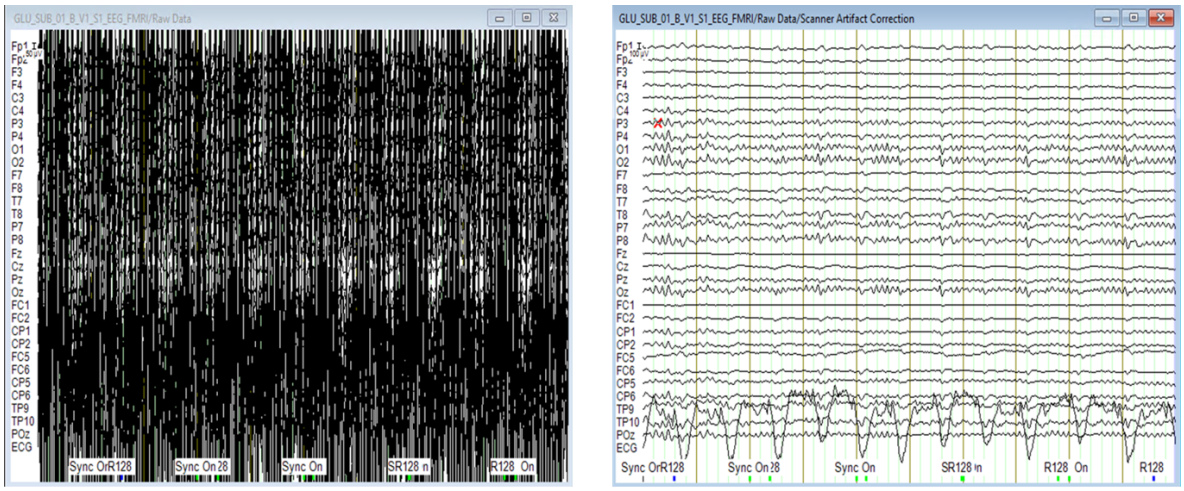

Figure 4.4: a) raw EEG data acquired simultaneously with fMRI. b) Pulse artifact corrected EEG

3.3.2 Band power analysis

Band power analysis was performed by an open-source MATLAB-based toolbox, Brainstorm (www://neuroimage.usc.edu/brainstorm) [121]. After artifact removal, cleaned data was imported into the brainstorm. All the data was trimmed into a fixed length of 9 minutes and 15 seconds to avoid possible harmonical artifacts at the beginning and end of the fMRI sequence. To evaluate the EEG signals' power in different frequencies, the power spectral density (PSD) was calculated with a window length of 2 seconds and no overlap ratio. Brainstorm uses the Welch method, a robust method for analyzing finite signals, to estimate the PSD. It involves dividing the signal into overlapping or non-overlapping segments and applying a window function in the time domain to each segment to reduce the spectral leakage. Then, the periodogram will be computed for each segment. The individual periodograms will be averaged to improve the overall estimate of the PSD, enhancing the signal-to-noise ratio and providing a smoother representation of the signal's frequency content.

Samples of PSD can be found in Figure 4.5. Afterwards, the PSD was extracted and used in a MATLAB script for band power analysis. Band power analysis is a common EEG analysis approach where the signal's average power in different frequency bands will be measured. These

bands are composed of delta (0.1-4 Hz), theta (4-7 Hz), alpha (8-12 Hz), beta (12-30 Hz), and gamma (32-100 Hz).

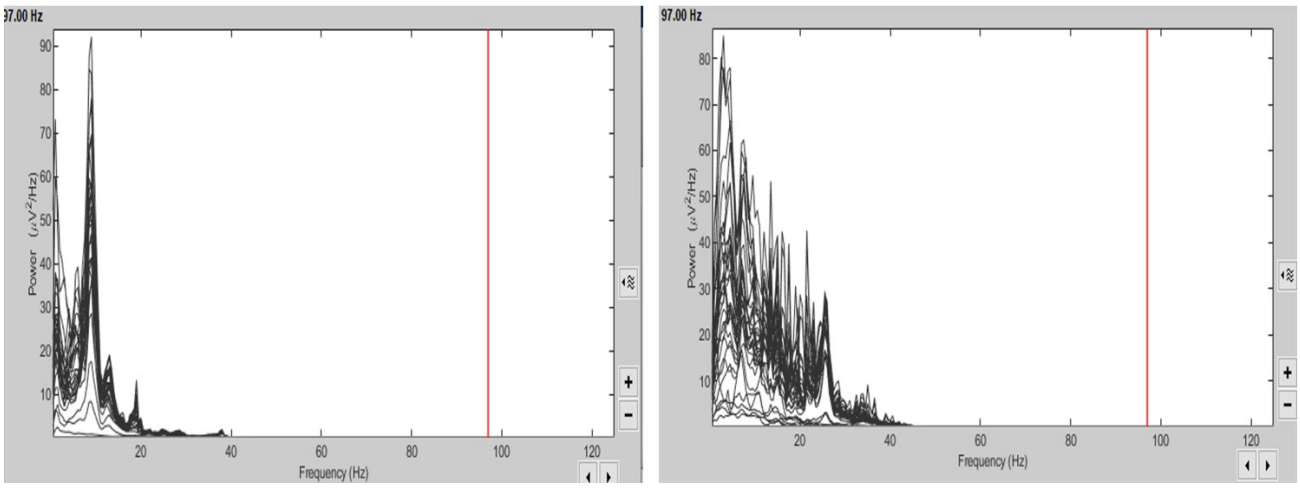

Figure 4.5: Power spectral density (PSD) samples

3.4 Functional MRI data analysis

Functional MRI data is often acquired in DICOM (Digital Imaging and Communications in Medicine) format (.dcm), which is a standard for the storage and transmission of medical images and their related information. It consists of a series of 2D images (slices) acquired over time during the fMRI scan, each representing a spatial snapshot of the brain activity. This comprehensive documentation also contains important information such as patient information, imaging parameters, and scanner settings stored in its header. It is common to convert DICOM to other formats, such as Analyze (.img and .hdr), or NIfTI (.nii) for analysis. Here, we used SPM12 (statistical parametric mapping) software to convert the DICOM data into the NIfTI format. SPM is a free, open-source, MATLAB-based package commonly used for analyzing fMRI, EEG, MEG, PET, and SPECT.

3.4.1 Preprocessing

Before we proceed with analyzing the fMRI data, we need to tackle the different artifacts that disturb the data such as head movement and temporal offset. In the following section, we will discuss the necessary preprocessing steps in detail. All the preprocessing steps are implemented

using SPM12 custom-designed scripts.

1) Removal of the first scans:

At the beginning of the acquisition, before the stabilization of the fMRI signal, the first recorded images may be contaminated by artifacts. As a result, they exhibit a higher signal level than the subsequently recorded images. These initial images need to be discarded to avoid skewing the study results. The removal of artifact-containing volumes was performed outside of SPM12 using a MATLAB script that removed the first few images.

2) Spatial realignment (motion correction):

Despite patients being instructed to avoid movement during the acquisition, small head movements or even respiration-caused movements are inevitable. The primary consequence of head movements is that a given voxel may not consistently occupy its original position across all the slices throughout the entire scanning period. To alleviate this motion impact, rigid-body transformations, including translation and rotation, are employed to spatially align the slices [122].

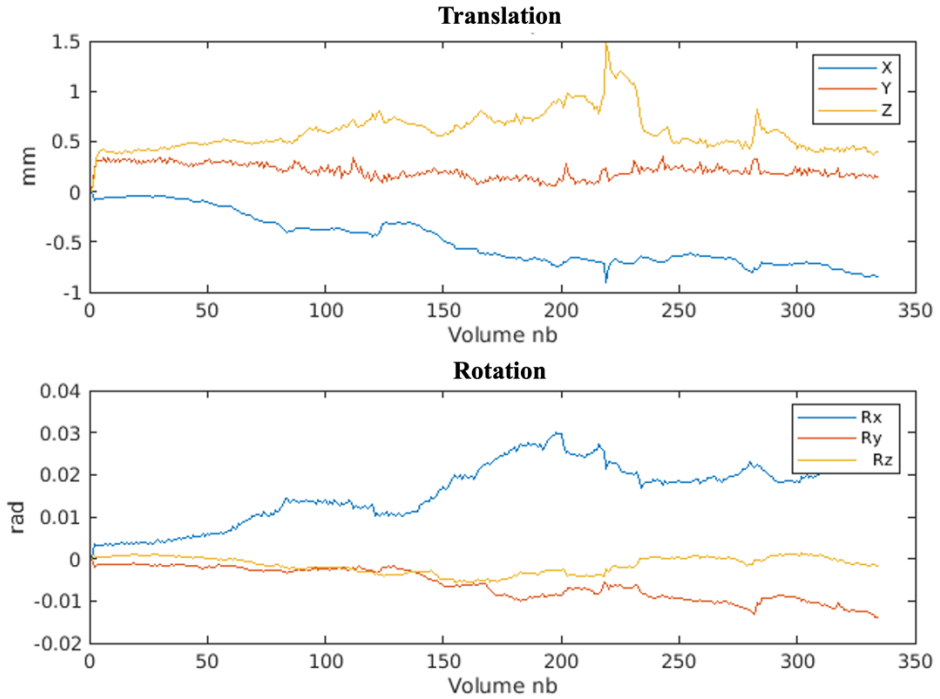

Figure 4.6: Estimated transformation for motion correction

The algorithm involves taking one image as a reference (fixed image) and transferring the other images (moving image) to spatially align them with the reference. Subsequently, through iterative optimization, the transformation parameters are adjusted to achieve the best alignment, ensuring spatial consistency in the analysis. As illustrated in Figure 4.6, the overall movement of images was confined within the interval of (-2 mm, 2 mm), which is half the size of the fMRI voxel. This suggests that there were no abrupt or extensive movements of the head. Otherwise, volumes affected by significant motion should have been excluded.

3) Slice timing correction:

In fMRI data collection over each TR (time repetition), 2D slices are acquired sequentially rather than simultaneously, leading to a lack of temporal alignment among them. This misalignment conflicts with the later assumption during modelling that all slices are collected simultaneously. Slice timing correction is employed to address this issue and to increase the statistical power, aiming to synchronize the temporal representation of bold fMRI changes across slices. In this correction process (Figure 4.7), a specific time point will be chosen as a reference and slices will be temporally adjusted to the reference by interpolation [123]. We chose the time point associated with the middle slice as a reference for the temporal alignment.

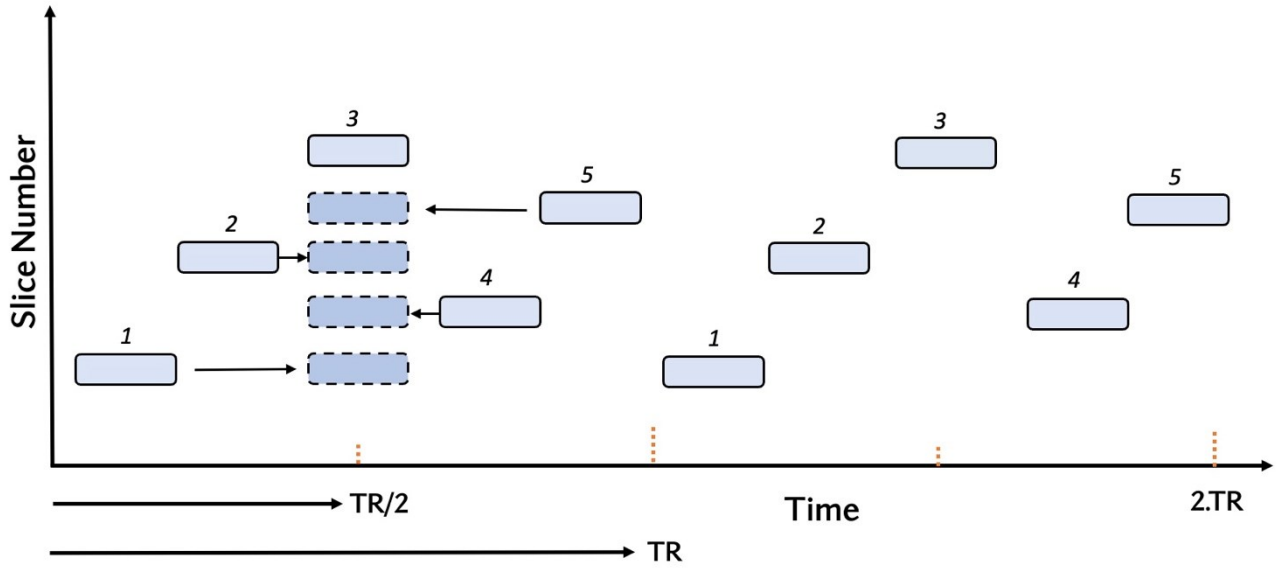

Figure 4.7: Slice timing correction

4) Spatial coregistration:

Coregistration employs a similar algorithm to the realignment process, but it focuses on aligning the images acquired from two different modalities, typically anatomical images and functional ones. High-resolution anatomical images, such as T1-weighted images, provide detailed structural information, while functional images with a lower resolution, such as BOLD images, capture dynamic changes in blood flow associated with neural activity. Coregistration ensures that anatomical and functional images are aligned and share a common coordinate space so that the corresponding anatomical and functional structures match accurately [124]. This process is essential for accurate analysis and interpretation of brain activity. Coregistration is often implemented in two subsequent steps: estimation and reslicing.

In the estimation part, the orientation of images will be adjusted to align one to the other. Instead of individually aligning several BOLD images with the anatomical image, a more robust approach is commonly taken in which the average of all the bold images will be aligned with the T1 anatomical image. The averaging improves signal-to-noise ratio in the moving image, leading to enhanced registration accuracy and ultimately contributing to more dependable results in image processing. After the necessary transformation is estimated, the reslicing process is performed. In reslicing, the moving image data resolution will be adjusted to match the reference and ensure each voxel possesses the same coordinate in both images.

5) Spatial normalization:

While the fundamental structure of every individual's brain is comparable, there is a slight variation in the size and morphology of different brains. Normalization is a crucial step in group studies that aims to bring all brain images into a standardized 3D space, allowing for meaningful comparisons across different subjects. This involves warping the functional images to an anatomical atlas, which serves as a standard reference for brain anatomy [125]. However, because of the relatively low resolution of functional images, it is conventional to warp the anatomical images to the template and then apply the same transformation to the functional images. To spatially warp the images to the chosen template, an affine transformation is utilized which is a combination of translation, rotation, zoom, and shear. Spatial normalization was not utilized in this study since the primary goal was to inspect the data at the subject level.

6) Spatial smoothing:

Smoothing is a common step in fMRI preprocessing which aims to reduce the high-frequency artifact by applying a spatial low pass filter, typically a Gaussian kernel, to the functional images. Besides enhancing the signal-to-noise ratio (SNR), smoothing will cope with small anatomical variability that is not compensated by spatial normalization. Therefore, it will increase the chances of capturing an activity as it spreads the activity through the neighbouring voxels. Smoothing comes with a trade-off of blurring spatial details, potentially compromising the precise localization of activations. Therefore, choosing the optimal degree of smoothing is of great importance, a determination that can be made based on the size and standard deviation of the smoothing kernel [126].

3.4.2 Extraction of bold time series:

Through the data acquisition, the two regions of interest (SMA and PCC) were defined as boxes within the anatomical space. As depicted in Figure 4.8, these boxes were transformed into labelled mask volumes. During coregistration, these masks were resliced and projected onto the functional volume to enable the extraction of their corresponding signals. Bold signals were then obtained by averaging the time series of all the voxels within each ROI. To further enhance the signal quality, regression analysis was applied to remove potential confounding variables, including quadratic drifts, motion parameters, averaged signals from the ventricular and white matter, and the global brain signal [127].

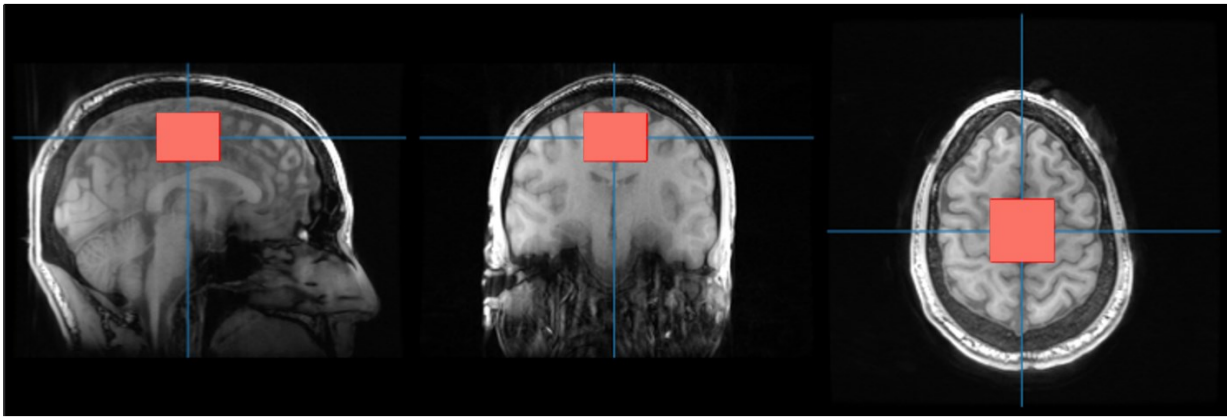

Figure 4.8: SMA labelled mask.

3.5 Statistical analysis

This section will provide details on statistical analysis performed on MRS results.

3.5.1 Shapiro-Wilk test

Shapiro Wilk test is a statistical test used to assess whether a given sample follows a normal distribution. Normality is a crucial assumption for parametric statistical tests, such as t-tests and ANOVA. This test compares the observed sample to what is expected under the normality assumption. The null hypothesis of the test states that the population from which the sample is drawn follows a normal distribution. The alternative hypothesis is that the population does not follow a normal distribution.

Let $X_1, X_2, \ldots, X_n$ denote a sample of size n from the population. Then, the Shapiro-Wilk statistic is calculated as follows:

$$W = \frac{(\sum_{i=1}^{n} a_i X_{(i)})^2}{\sum_{i=1}^{n}(X_i - \bar{X})^2} \quad (1)$$

In the abovementioned equation, a_i represents test-specific constants which can be computed from the sample. X_i, $X_{(i)}$, and $\bar{X}$ show the i-th observed sample, the i-th ordered sample, and the sample mean, respectively [128].

If the test statistic is significantly different from what would be expected under a normal distribution, the null hypothesis will be rejected concluding that the sample does not follow a normal distribution. However, if the p-value is not less than the significance threshold, we can infer that there isn't sufficient evidence to reject the null hypothesis.

While applying the Shapiro-Wilk test to our sample data, the null hypothesis was rejected for certain samples due to either the small sample size or the possibility that the sample is not actually derived from a normal distribution. Hence, we proceeded with the rest of the statistical analysis with non-parametric tests suitable for cases when either the normality cannot be assumed or when the data is not normally distributed.

3.5.2 Wilcoxon Signed-Rank test:

The Wilcoxon Signed-Rank test is a non-parametric statistical test designed to assess whether there is a significant difference between two paired samples. This test is an alternative to the parametric paired t-test. This test operates based on evaluating the distribution of the signed differences between paired observations.

The Wilcoxon Signed-Rank test involves calculating the differences between paired observations and assigning ranks to these differences based on their absolute values. For tied ranks the average rank will be calculated. Then, positive and negative ranks are assigned to positive and negative differences, respectively. The test statistic is determined by summing the ranks of either the positive or the negative differences, depending on which sum is smaller. Ultimately, the test statistic is compared to critical values from the Wilcoxon Signed-Rank table or converted into a p-value to determine the statistical significance. If the test statistic falls outside the critical region defined by a chosen significance level, the null hypothesis is rejected, implying a statistically significant difference between the paired samples.

In this experience, Wilcoxon Signed-Rank was employed to assess the statistical significance of the observed difference in glutamate concentrations between two different time points of the visit.

3.5.3 Friedman test:

The Friedman test is a non-parametric statistical test designed to evaluate whether there are significant differences among multiple related groups or measurements. This test is a counterpart of the repeated measures ANOVA, particularly when the assumption of normality is not met or when dealing with ordinal or non-normally distributed data.

In the Friedman test, data are collected from each subject under different conditions or at various time points, resulting in a set of related measurements. The procedure involves ranking the observations within each sample independently and calculating the average rank for each condition. The test statistic is then computed by assessing the differences in the sum of the ranks across the different conditions. Similar to the *Wilcoxon Signed-Rank test*, interpretation of the Friedman test involves comparing the calculated test statistic to critical values from statistical tables. If the test statistic exceeds the critical value at a chosen significance level, the null hypothesis is rejected, suggesting that there are significant differences among the related samples.

The Friedman test is often employed in studies where repeated measurements are taken from the same subjects under different conditions, like our study where glutamate concentrations are measured before, right after, and a while after learning a motor sequence.

3.5.4 Bootstrap method:

Bootstrapping is a statistical technique designed to address challenges posed by small sample sizes or when the underlying data distributions are uncertain. The key idea behind bootstrapping involves repeatedly and randomly drawing samples with replacements from the observed dataset, generating multiple bootstrap samples. This process allows us to estimate the distribution of a statistic of interest, such as the mean or median, relying on the characteristics of the observed data rather than any predefined assumptions on the population distribution.

In this study, we have conducted the aforementioned tests to assess whether the statistical significance of the observed data can be verified. However, statistical tests have limited power to detect true effects in a small sample size of five, and we were not able to draw strong conclusions about the significance of the observed effect. Therefore, in the next chapter, we will focus on a qualitative discussion of the findings.

Chapter 5 : Results and discussion

This chapter outlines the primary outcomes of the data analysis for each imaging modality. In each section, the preprocessing impact is illustrated on the data before delving into the data analysis Following the data analysis, the significance of the results will be conveyed based on the outcomes of the specified statistical analyses. The results will be assessed against the hypotheses to determine their alignment with expectations.

Additionally, a thorough discussion on interpreting the results and their alignment with existing literature will be presented. Any discrepancies between expectations and results will be explored, with possible explanations proposed. Since this study is an ongoing experiment, the results for some modalities are preliminary analyses, and more data is required for generalizing the observed outcomes to the entire population.

In summary, this chapter gathers findings to investigate the memory trace generated by motor sequence learning, specifically in two regions: the supplementary motor area (SMA) as the motor-implicated region and the posterior cingulate cortex (PCC) as a control region. To achieve this, simultaneous electroencephalogram (EEG)-functional magnetic resonance imaging (fMRI) was employed along with magnetic resonance spectroscopy (MRS). This integration of three modalities in a single experiment enabled an exploration of the relationship between brain metabolism, neuronal electrical activity, and the BOLD signal. Glutamate, obtained through MRS, served as a marker for metabolism and synaptic plasticity, while EEG and fMRI were utilized to assess variations in neuronal activity induced by learning. Performance measurements will be provided to observe the influence of learning on performance enhancement and to appropriately link the findings with different stages of learning. Moreover, the in-hand cortisol and melatonin measurements will be presented as additional factors for validating the outcomes as learning progresses.

5.1 MRS results (first approach):

5.1.1 FID-A preprocessing results:

As mentioned earlier, we employed two approaches to extract glutamate variations from the raw MR spectrum. In the first approach, we utilized FID-A for preprocessing the raw data. This involved tasks such as combining signals received from different coils, removing unreliable averages, performing frequency alignment, and applying phase correction.

As illustrated in Figure 5.1a, signals received by 32 different coils exhibit varying phases and signal-to-noise ratios (SNR) due to their relative locations with respect to the region of interest. To standardize these signals and make them comparable, proper complex weights must be calculated and applied to each signal. During this process, signals with higher SNR receive stronger weights, while those with lower SNR are assigned weaker weights. This step not only facilitates signal averaging but also optimizes the overall SNR. Figure 5.1b displays the spectra after the coil combination.

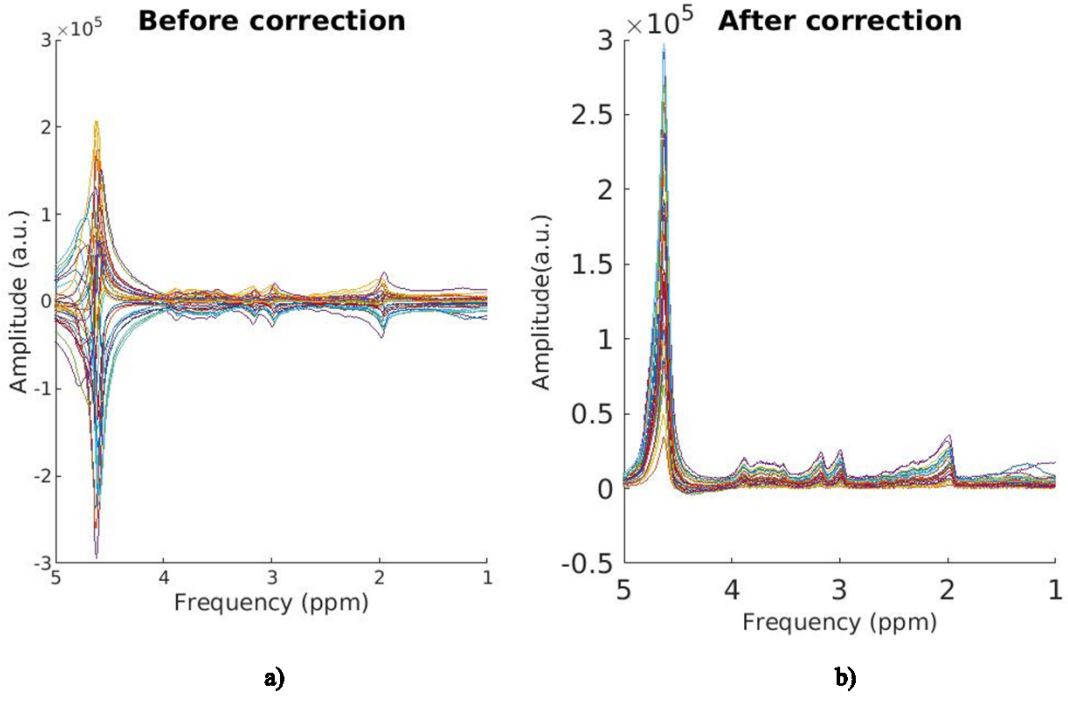

Figure 5.1: Signals before and after coil combination (Subject02/MSL day/ Session2/SMA region). a) Signals received by different coils at distinct locations with reference to the voxel of interest. b) Signals after applying the appropriate complex weights.

In the subsequent step, the removal of corrupted averages was followed by spectral alignment. Minor variations in the magnetic field or physiological factors, such as subtle movements like breathing, can introduce phase and frequency drifts in the spectra. Consequently, it is essential to estimate and correct these frequency and phase drifts to ensure the spectra are aligned. This alignment allows for averaging of the spectra, ultimately creating the main final spectrum. The preprocessing results, belonging to the data of the subject02 for the SMA region on the second session of the MSL day, our depicted in Figure 5.2.

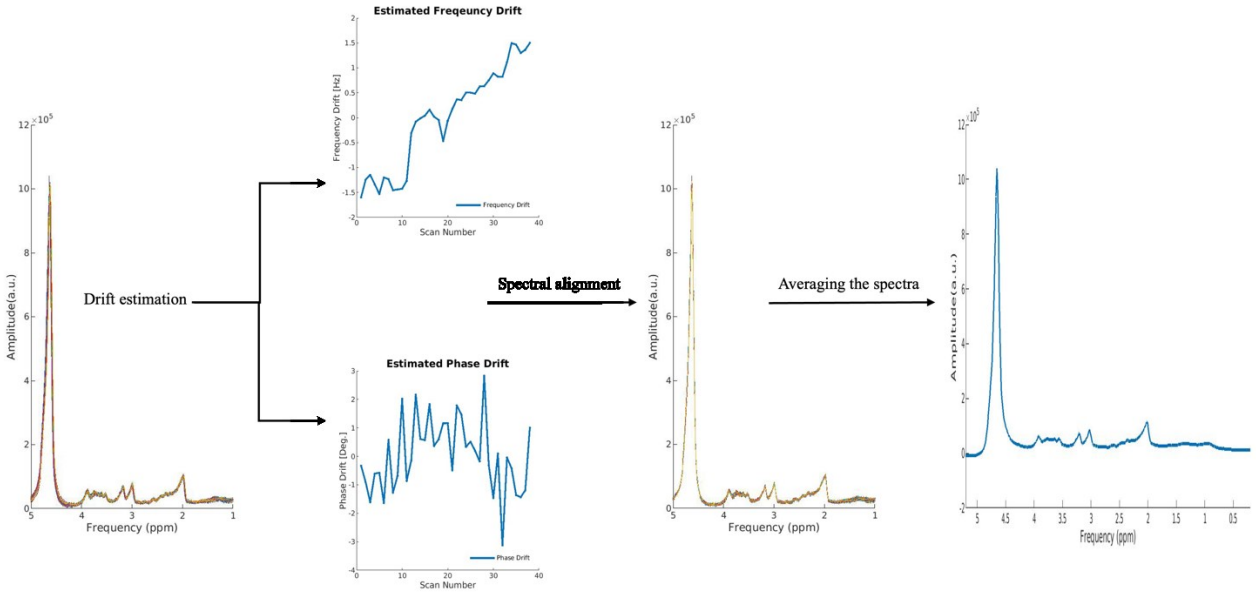

Figure 5.2: Preprocessing results obtained by aligning and averaging the spectra.

(Subject02/MSL day/Session2/SMA region)

5.1.2 Tarquin fitting results:

After preprocessing, the water-suppressed and water-reference data were fed into TARQUIN, using the input parameters specified in Table 1. TARQUIN then fitted the basis spectra set to the preprocessed spectrum, resulting in the generation of concentrations for various metabolites. The fitting results, along with glutamate contribution to the spectrum, for two subsequent sessions of subject05 MSL visit are shown in Figure 5.3. The data is acquired after the first MSL task, and an increase can be observed in the glutamate concentration.

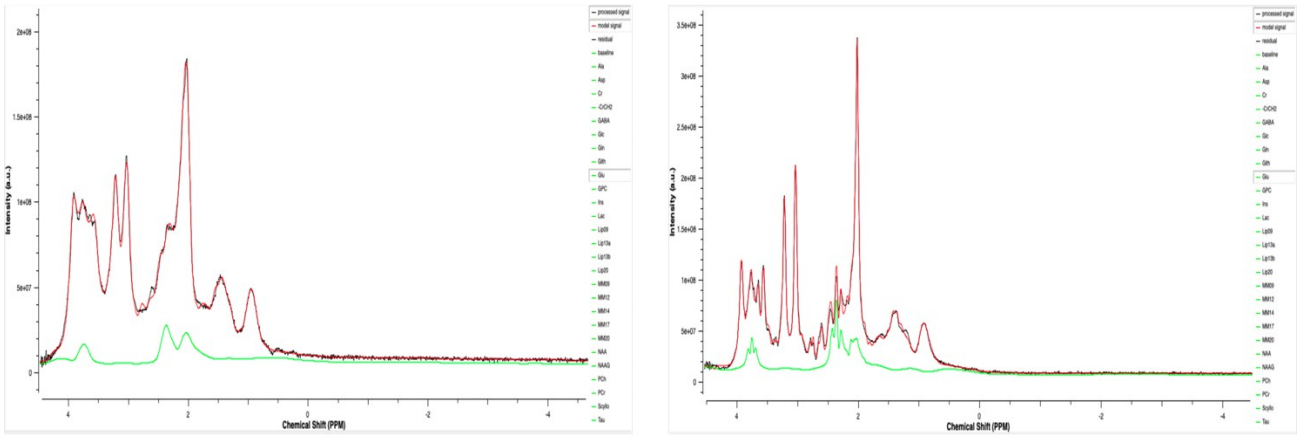

a) b)

Figure 5.3: The fitting results (red curve) with the contribution of glutamate (green curve) for two subsequent sessions. a) Subject05/MSL day/Session2/SMA region. b) Subject05/MSL day/Session3/SMA region

5.2 MRS results (second approach):

In the second approach, we utilized FSL-MRS to analyze the MR spectroscopy data. Similar preprocessing steps were executed to generate the spectrum of interest from raw data recorded by multiple coil receivers. These steps primarily involved coil combination, spectral registration, averaging, eddy current correction, and residual water peak removal.

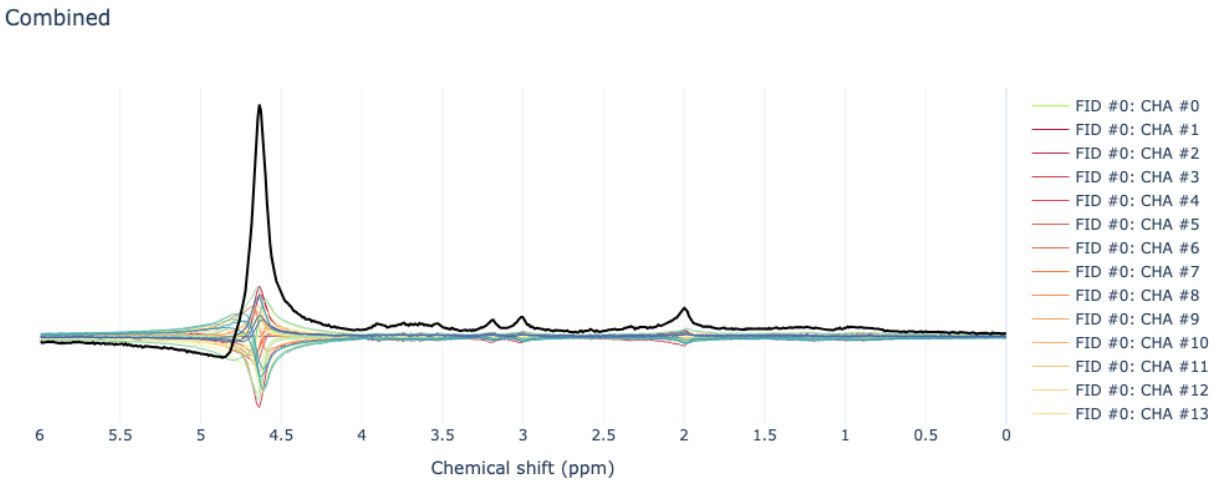

Figure 5.4: Coil combination in FSL-MRS (Subject02/MSL day/ Session2/SMA region).

Similar to the first approach, coil combination served as the initial step, unifying the signals from different coils into the same coordinate system, as illustrated in Figure 5.4. Subsequently, the residual

variations in phase and frequency were largely compensated for through spectral registration. Examining Figure 5.5 reveals a reduced misalignment in the spectra after this correction.

Finally, the spectra were averaged to create a single spectrum with an optimized signal-to-noise ratio (SNR). Figure 5.6 demonstrates that the averaged spectrum is notably affected by the water signal, despite the use of the CHESS sequence for water suppression. The water peak (depicted in red) was successfully removed using the HLSVD algorithm in FSL-MRS. It is evident that the influence of the water signal is minimized in the corrected spectrum (depicted by the blue curve) following the removal process.

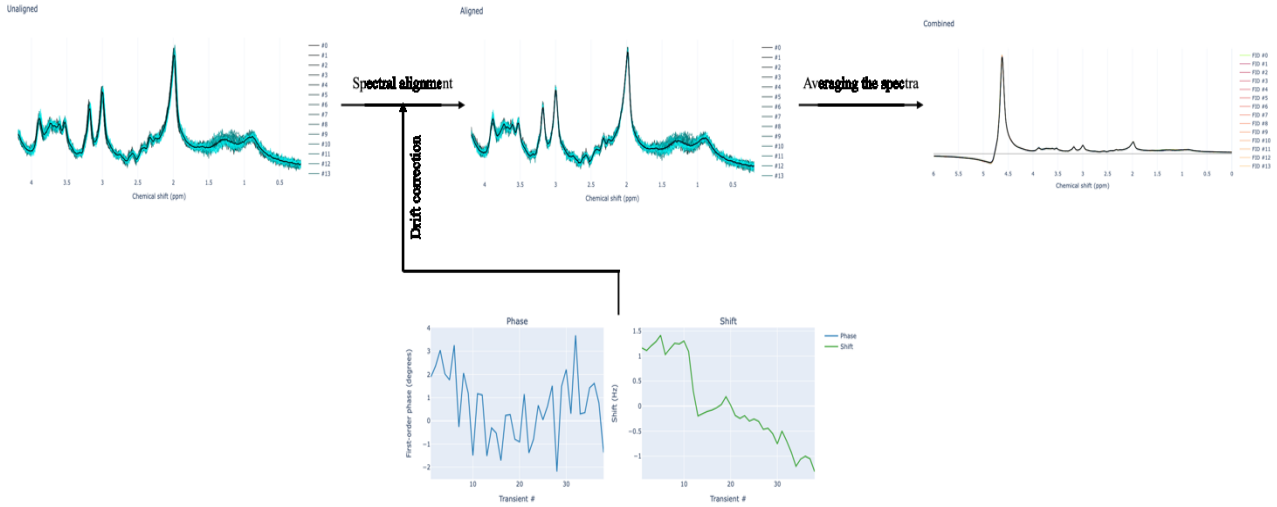

Figure 5.5: Aligning and averaging the spectra by FSL-MRS (Subject02/MSL day/ Session2/SMA region).

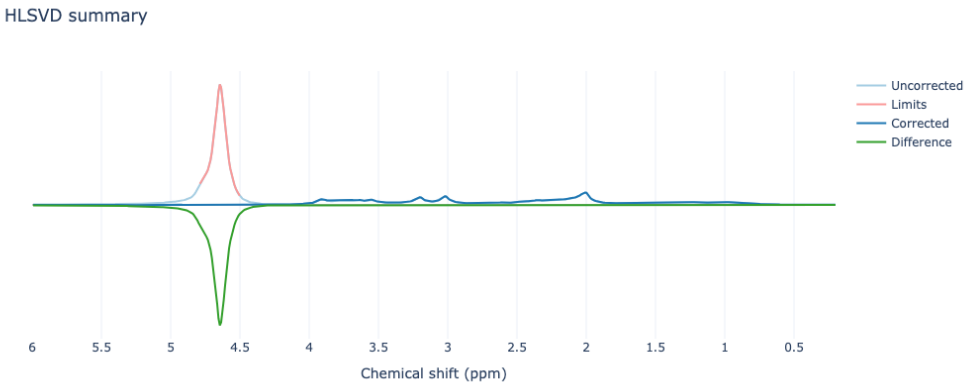

Figure 5.6: Residual water peak removal using HLSVD algorithm in FSL-MRS (Subject02/MSL day/ Session2/SMA region).

The fitting results were highly comparable to those obtained by TARQUIN, validating the reliability of the first approach. Therefore, moving forward, we will focus on the analysis of the results derived from the first approach.

5.3 Subject-level analysis

5.3.1 Diurnal changes in glutamate levels:

The dynamic variation in the glutamate concentration for each subject was examined across different sessions of their visits. Figure 5.7 illustrates this dynamic for Subject01. During the control day, for this specific subject, a gradual rise in glutamate concentration of the PCC region (motor control region) can be observed. The same ascending trend is noticeable in the SMA between the initial acquisition in the morning and the final acquisition at night. However, the variation pattern between each session in SMA seems to have a larger amplitude.

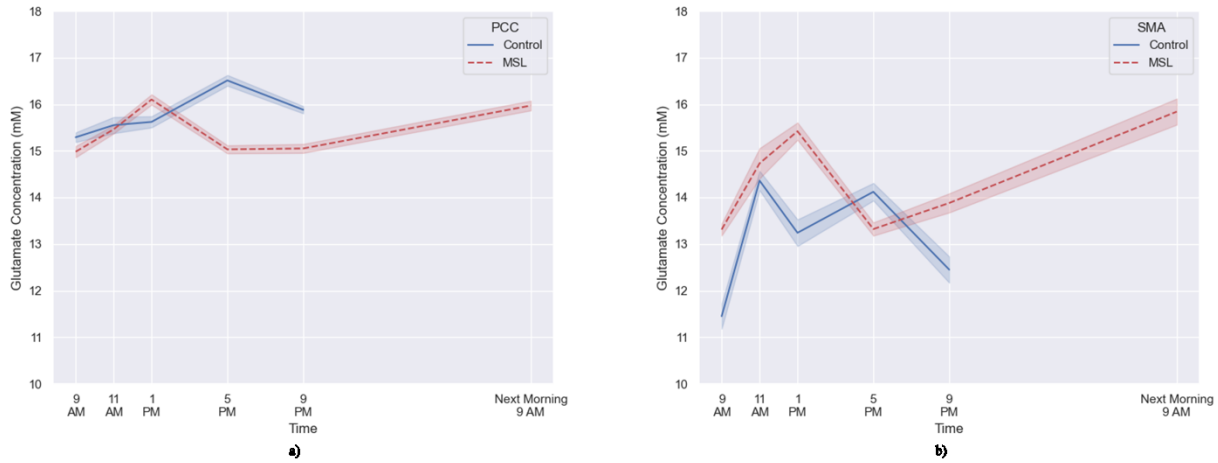

Figure 5.7: Diurnal glutamate variation on the MSL and control day (Subject01). a) PCC region. b) SMA region.

During the MSL visit, the patterns of glutamate dynamics differed from those observed on the control day. Following the initial learning of the MSL task, there is an increase in glutamate concentration peaking approximately two hours after learning. This peak is followed by a return to the baseline after a few hours of wakeful rest. Upon exposure to the MSL task for the second time during a recall session, right before the 5 pm scan, there is a subsequent rise in glutamate concentration. The observed pattern is evident in both the SMA and PCC; however, PCC appears to exhibit a scaled-down version of the

fluctuation observed in SMA. In addition, the baseline level of glutamate in PCC is observed to be generally higher than SMA on both days, which can be justified by the high metabolic rate of PCC serving as a fundamental component of the default mode network (DMN) [129].

As mentioned earlier, several studies indicate a reduction in glutamate levels post-sleep, particularly during the non-rapid eye movement (NREM) stage [54], [55]. Interestingly, in the case of this specific subject, the glutamate levels fail to return to the baseline after a night's sleep, contrary to expectations. Upon examining the cortisol level data presented in Figure 5.8, we propose that the elevated glutamate concentration in the morning scan might be linked to the increased cortisol level compared to the baseline.

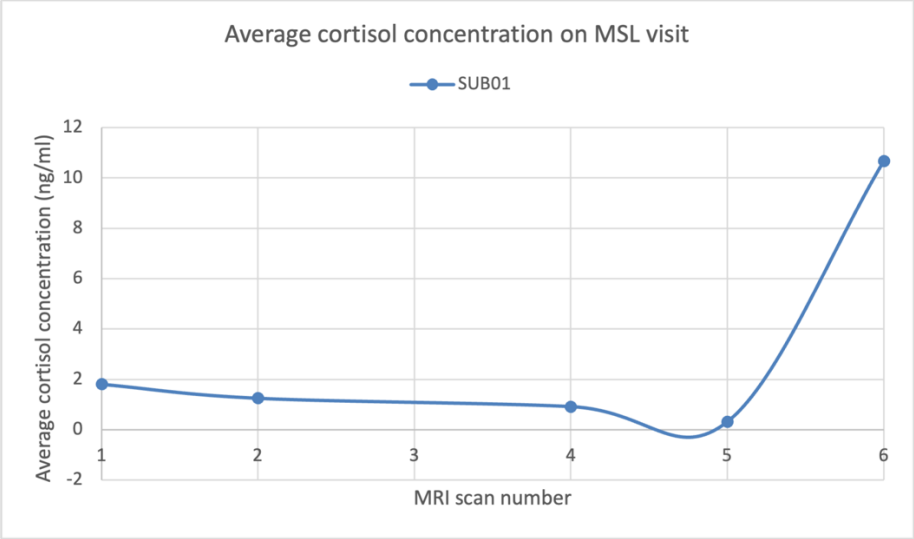

Figure 5.8: Cortisol concentration measurements for Subject01 (MSL visit)

Cortisol serves as the primary glucocorticoid in humans and is commonly known as the 'stress hormone.' While human cortisol levels usually exhibit a circadian rhythm, being higher in the early morning to facilitate wakefulness and lower in the evening to support sleep [130], studies indicate that exposure to glucocorticoids in the short term can impact glutamate transmission, leading to an elevation in extracellular glutamate concentration [131], [132].

We also examined melatonin measurements for any abnormalities. Melatonin, mainly synthesized by the pineal gland, is an essential hormone for circadian rhythm regulation. Melatonin levels gradually rise in the early evening as it gets dark, reaching peak levels during the middle of the night [133].

Upon reviewing the melatonin measurements of Subject01, a rising trend in average concentrations is observed from 4 pm onward, with no distinguished irregularities.

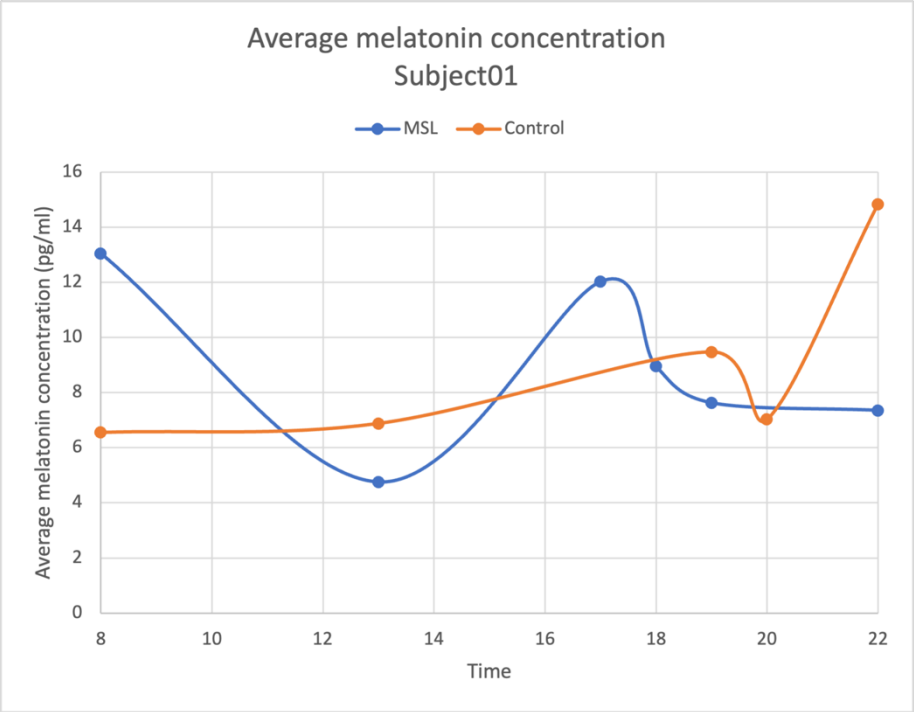

Figure 5.9: Melatonin concentration measurements on the MSL and control day for Subject01

5.3.2 EEG analysis:

In the same recording session as the glutamate acquisition, EEG was conducted to investigate learning-specific modulation in neuronal oscillation. When analyzing the EEG signals, our attention was directed towards electrodes in close proximity to our regions of interest. We linked the FC1, FC2, C3, and C4 electrodes to the SMA region, and P3, P4, CP1, and CP2 electrodes to the PCC region. Examining the EEG power of Subject01 across different frequency bands reveals two subsequent peaks. Initially, a significant increase in power is evident in the corresponding electrodes of both regions a while after the initial exposure to the MSL task, specifically during the 1 pm scan. This increase in power suggests neuronal synchronization, likely facilitating the formation of memory traces that are induced by the MSL task. After the initial exposure of the participant to the new motor sequence task, the brain is expected to exhibit heightened neural activity, reflecting the engagement of cognitive processes for learning the novel sequence.

The second peak emerges after practicing the MSL task for the second time during a recall session. This peak is characterized by a lower amplitude, suggesting neural adaptation that enables the brain to optimize its resources for processing new information. With a repeated performance of the same motor task, neural circuits involved in the task become optimized for efficient coordination and execution of the sequence elements. Additionally, the participant will have a few hours of wakeful rest between the first and second MSL sessions. As mentioned earlier, during this period when cognitive demand is lower, initial consolidation takes place, refining and stabilizing neuronal representations [57]. This process is often linked to improved performance and increased efficiency in motor skills. All things considered, the cognitive load associated with performing the motor sequence decreases as the task transitions from an explicit, conscious phase to a more implicit, automatic manner, resulting in a relatively lower EEG power modulation.

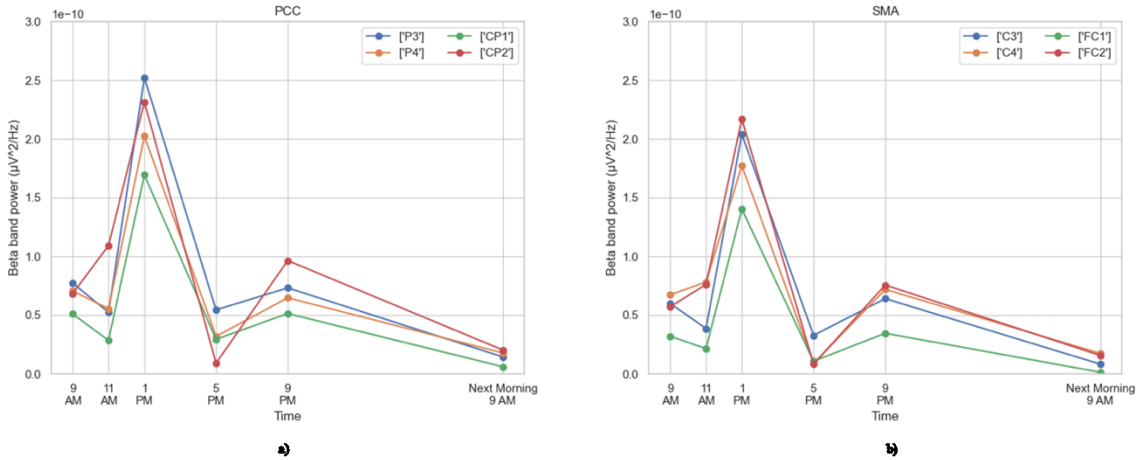

Figure 5.10: Average beta band power for Subject01.

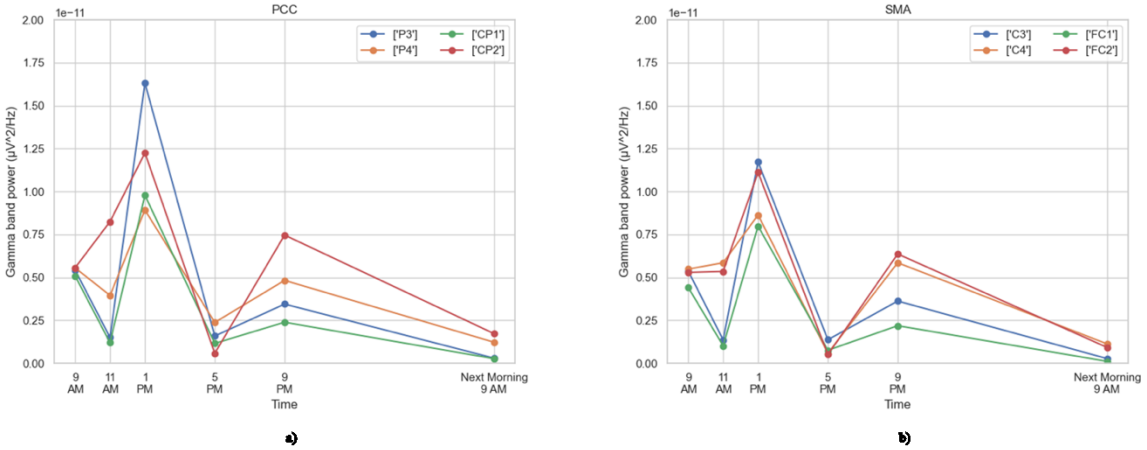

Figure 5.11: Average gamma band power for Subject01.

Interestingly, this modulation was observed in the average power of the EEG signal, as well as in the average power of all frequency bands of electrodes of interest. No particular frequency band was found to be more engaged in the process. Figure 5.10 and Figure 5.11 illustrates average beta and gamma band power, respectively.

5.3.3 Functional MRI BOLD signal:

Functional MRI images were analyzed to evaluate learning-induce variation in blood-oxygen-level-dependent (BOLD) signal. The BOLD signal serves as an indirect indicator of neural activity. To quantify and compare neural responses across different sessions and conditions, the area under the curve (AUC) of the BOLD signal was introduced as a summary measure.

Figure 5.12 presents the AUC of the BOLD signal across different visits, revealing a distinct modulation in neuronal activity during MSL compared to the control condition. Following the initial MSL session, both regions exhibit an elevated BOLD signal intensity. The PCC shows a gradual increase that persists for a while after training which may reflect an ongoing cognitive processing during rest. In contrast, the SMA displays a transient, abrupt peak in signal intensity which is only observed right after the session.

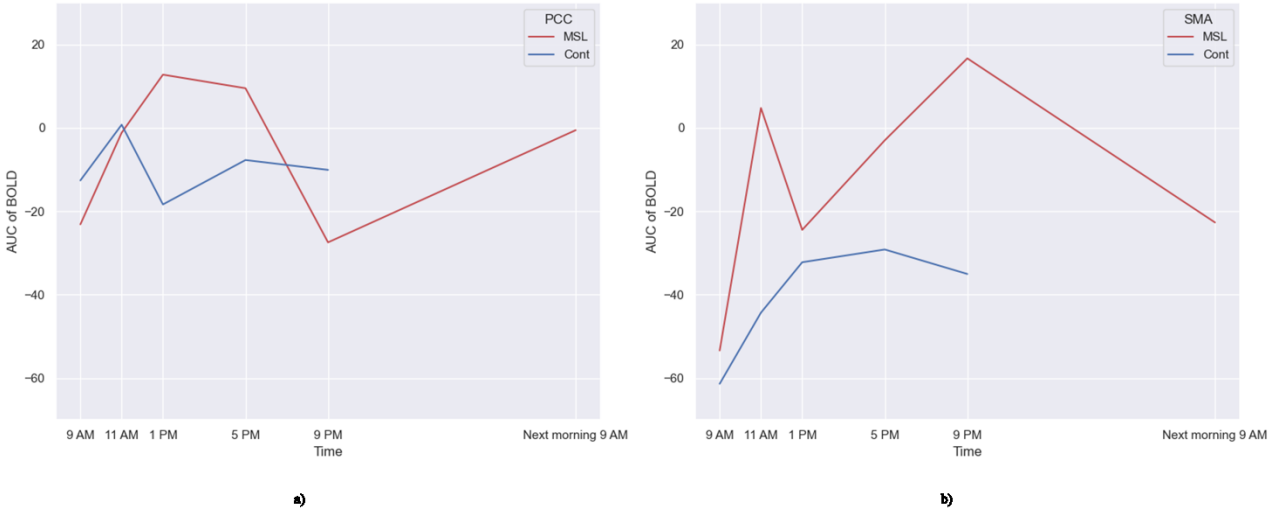

Figure 5.12: Area under the curve (AUC) for BOLD signal on the MSL and control day (Subject01).

a) PCC region. b) SMA region.

The second MSL session induces a lasting increase in the SMA's BOLD signal possibly reflecting neuroplastic changes associated with the repeated practice of the motor sequence. Conversely, PCC's bold signal returns to baseline level by the last scan of the day (9 pm), suggesting that this region is less actively engaged during the later stages of learning. This finding is consistent with the model proposed by Doyon and Benali [126] suggesting that basal ganglia and associated motor cortical regions (SMA) are solely involved in the latest stage of learning.

Matching the BOLD variation with the outcome of EEG analysis shows that our results align with the findings of Logothetis and Laufs [134], [135], indicating that there is a link between EEG power and fMRI BOLD signal. Additionally, we can confirm that BOLD signal variation is probably linked to the execution of motor sequences and the intracortical processes in the region of interest rather than its spiking output [134].

5.4 Group-level analysis

5.4.1 Performance duration:

As previously mentioned, skill acquisition progresses through different stages. The initial stage is characterized by rapid and significant performance improvement occurring within the initial session. The subsequent performance improvement occurs gradually across multiple sessions of practice. To investigate the learning process and assess skill acquisition, performance durations were recorded across three MSL sessions: 1) an initial learning session, 2) a recall session on the same day, and 3) a recall session on the next day following an overnight sleep.

Figure 5.13 shows the average performance duration through each MSL session. As expected, a substantial decrease in performance duration is evident during the first MSL session. Over the next two sessions, performance improvement is gradual and subtle. On average, the first execution of the sequence in the second MSL session is completed more rapidly than the last sequence in the initial MSL session. This progress in performance reflects the consolidation of memory occurring during the rest period between practice sessions. The same effect can be observed between the same-day and the next-day recall session. On average, participants' performance improved between the two sessions without practicing the sequence. The second between-session performance improvement also reflects memory consolidation during sleep. In addition to the average improvement, a notable reduction can be observed in the variability of performance durations among different subjects. Initially, individual

differences led to high variations in the performance duration of the participants. However, as the learning progressed neuronal circuits were refined, optimized, and stabilized, leading to a decrease in performance differences among subjects.

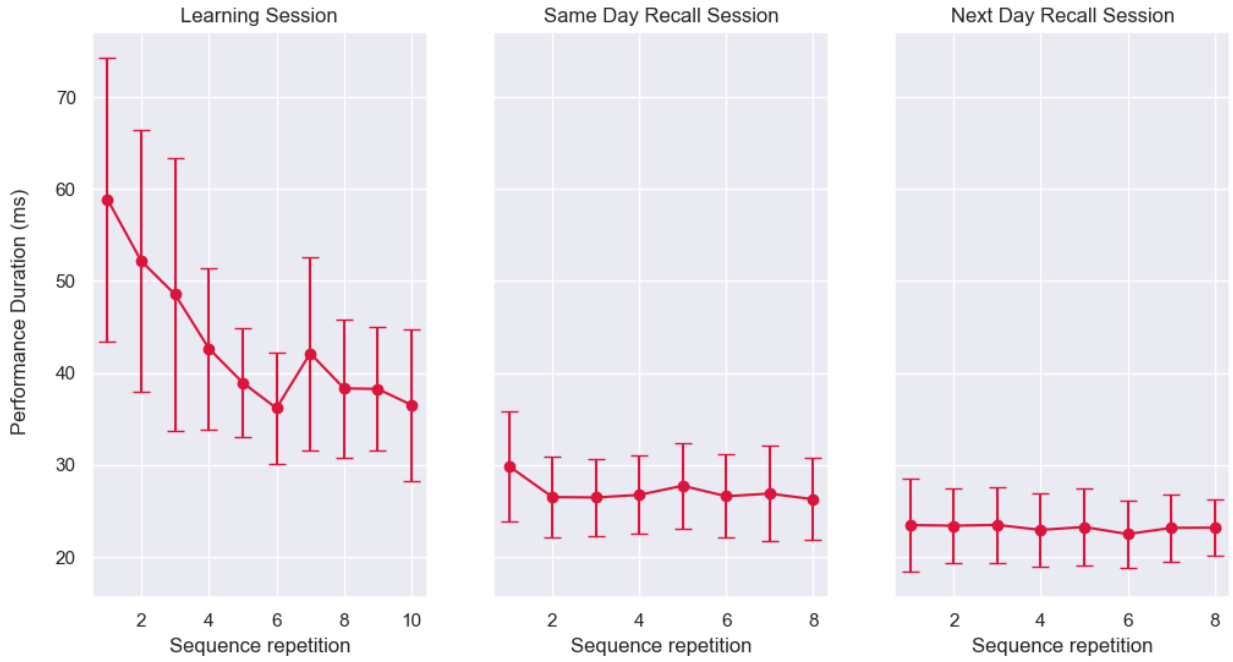

Figure 5.13: Performance duration for each MSL task session.

5.4.2 Average glutamate changes:

Now that we have analyzed and integrated data from different modalities for the first subject, we will proceed with the group-level analysis of the MRS data. It has been shown that memory traces are primarily created through glutamate-mediated processes. Therefore, we have chosen glutamate concentration as a marker to investigate these memory traces. We have previously reported our findings on a single subject, and now, to generalize the results to the entire population, the variation in group average glutamate concentration should be assessed. As previously noted, this study is still ongoing; nevertheless, in this section, we will present the analysis results for the so far data collected from five young healthy individuals.

Figure 5.14 illustrates the glutamate concentrations averaged across all participants. On the control day, a trend toward higher values is observed during the day for both regions. This rise is consistent with existing animal studies suggesting an increase in glutamate levels during the wake periods [47],

[55], [136]. The mentioned increase is also evident on MSL day; however, it appears through a different pattern. Between 11 am and 1 pm, after the first MSL session, there is an increase in glutamate, which is sustained until 5 pm. After the second MSL session, a slighter increase can be seen from 5 pm to 9 pm. During both conditions, the glutamate variation in PCC seems to be more subtle compared to SMA. Although both regions are approximately following the same pattern, PCC seems to be following a downscaled variation.

Upon analyzing the variation in glutamate during the control visit, it appears that, at certain points after reaching a specific level, glutamate concentrations are modulated to a lower level. Additional investigation is required to discuss the underlying reason for this phenomenon. Contrary to expectations, although glutamate levels have descended after a night of sleep following the MSL day, they are not restored to the baseline value. This can be due to the fact that glutamate regulation is a complex process influenced by various factors such as neuronal activity, synaptic plasticity, and circadian rhythm.

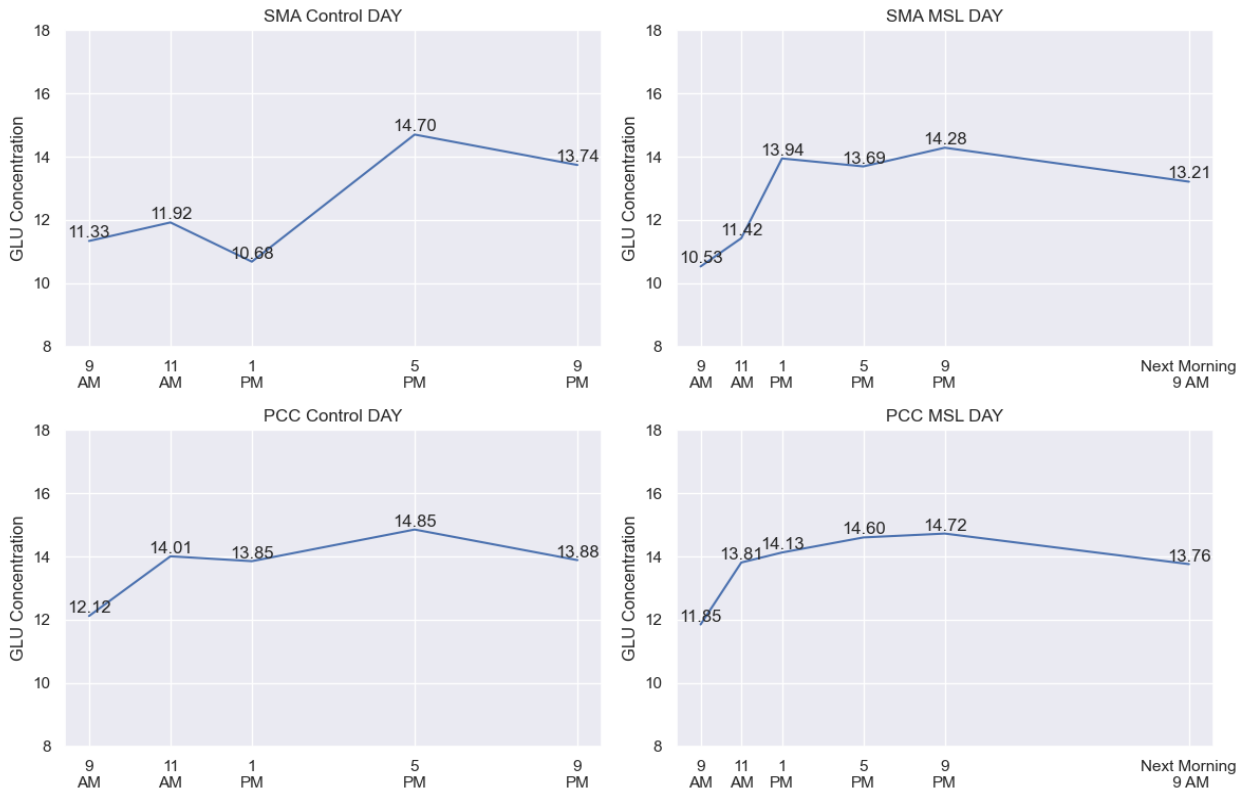

Figure 5.14: Group averaged glutamate concentrations in SMA and PCC

To differentiate learning-induced glutamate modulation from other factors, such as circadian regulation of glutamate, we assessed the normalized glutamate concentration with respect to the control session. Figure 5.15 shows the difference between the glutamate dynamics of the MSL visit and the control visit. After learning the MSL task in the first session, a significant increase is observed in the normalized data of the SMA region, indicating memory consolidation along with its underlying synaptic plasticity and neuronal circuit refinement. Additionally, a subsequent decrease to the baseline level is followed by a slight increase after the second MSL session, possibly contributing to further consolidation of the memory. When comparing the glutamate variation in the PCC region between the MSL and control sessions, there is no significant modulation; however, the same tendency may be observed with a much lower amplitude.

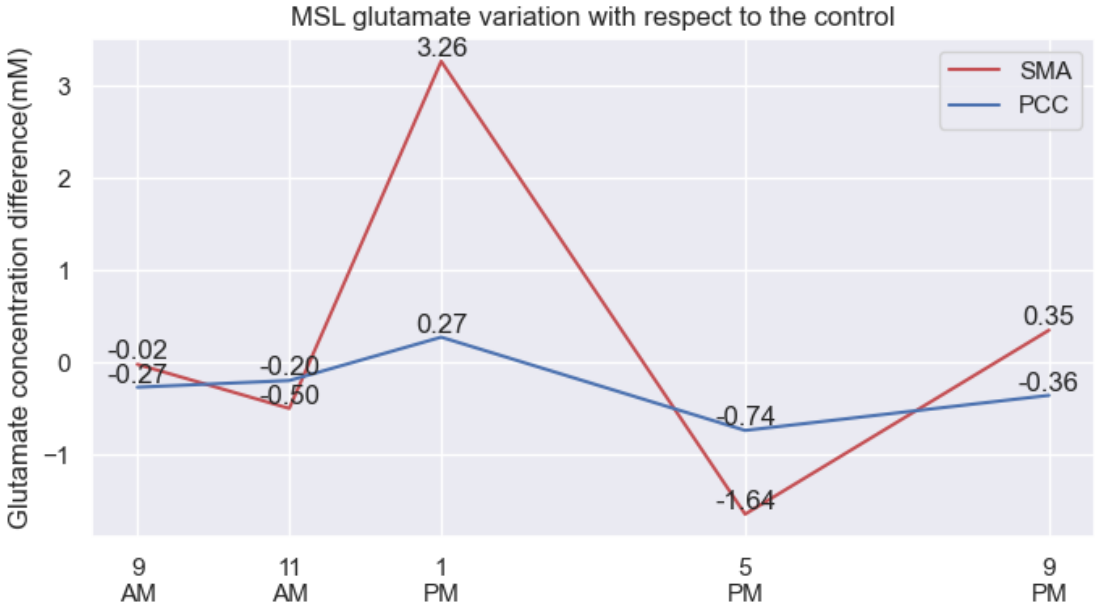

Figure 5.15: Glutamate concentration on MSL day normalized with respect to the control day.

Chapter 6 : Conclusions and future work

6.1 Concluding remarks

The main findings of this study can be summarized as follows.

- The performance measurement confirmed that skill acquisition is divided into multiple phases. The significant decrease in the performance duration of each sequence over the first MSL session indicates the fast phase of learning, which makes up most of our performance. The slow phase of learning is characterized by slight performance improvement across sessions, while the performance gain between sessions, without practicing the sequence, reflects the memory consolidation process.
- Glutamate regulation is a complex process influenced by several factors, including circadian rhythm, stress, hormone levels (particularly cortisol and melatonin), neuronal activity, and synaptic plasticity. Therefore, interpreting the variation in glutamate concentration should be done with caution.
- On the control visit, the group-averaged glutamate concentration showed an increasing tendency during wakefulness, which is consistent with previously conducted animal studies.
- The findings from the group-averaged glutamate concentration on the MSL visit indicate that motor sequence learning is accompanied by an increase in the glutamate concentration of the supplementary motor area (SMA). This result suggests that motor learning and memory formation occur through glutamate-mediated processes mainly in the motor-implicated areas.

  Additionally, an overnight reduction in the glutamate concentration was observed after the overnight sleep session, possibly as a result of sleep homeostasis processes.
- The integration of the first subject's data from different modalities suggests that the variation in glutamate concentration modulates the neuronal activity assessed by EEG and fMRI. Upon examining the variation in glutamate concentration, the power of the EEG signal, and the BOLD signal area under the curve one may find the tight coupling between neuronal activity, metabolism, and cerebral blood flow.

6.2 Future work

Although this study provides valuable insights into how motor memory traces are formed through glutamate-mediated processes, further investigation is required to comprehensively study the underlying mechanism of motor skill acquisition.

- More data needs to be collected and analyzed from eligible participants to increase the statistical power and generalize the study findings to the entire population of young, healthy adults.
- The polysomnography (PSG) data needs to be analyzed during different stages of sleep to explore sleep homeostasis and memory consolidation processes and their effect on the glutamate concentration and the neuronal activity observed in the next morning scan.
- The collected EEG-fMRI data suggests that other regions may also be involved in the learning process. Therefore, as a future work, the EEG-fMRI data will be analyzed over the entire brain to extract the large-scale functional network involved in different stages of skill acquisition.
- So far, we have collected resting-state EEG-fMRI on 6 time points during the MSL visit, two of which were collected a few minutes after being exposed to the MSL task. In the next stage, EEG data will also be recorded during the MSL task to explore the simultaneous modulation in neuronal activity, possibly revealing the role of a specific frequency band in learning.
- To regulate the neural activity in the CNS, glutamate works in a complementary manner with GABA, an inhibitory neurotransmitter in the CNS. Exploring their interplay is essential for unravelling the complexities of neural regulation. Furthermore, we hypothesize that glutamate and GABA concentrations can be particularly used as two main sources in modelling the fMRI bold signal. To assess this complementary work, another MRS sequence, called MEGA-PRESS, should be implemented to measure GABA concentration. Therefore, in the next phase of the study, we may employ this sequence to measure GABA concentrations.
- As glutamate concentrations in the brain are relatively low compared to other metabolites such as lactate, we may continue the data acquisition using a 7T MRI scanner to increase the sensitivity to the variation of glutamate levels.

References

[1] L. G. Ungerleider, J. Doyon, and A. Karni, "Imaging brain plasticity during motor skill learning," *Neurobiol Learn Mem*, vol. 78, no. 3, pp. 553–564, Nov. 2002, doi: 10.1006/nlme.2002.4091.

[2] I. Tavor, R. Botvinik-Nezer, M. Bernstein-Eliav, G. Tsarfaty, and Y. Assaf, "Short-term plasticity following motor sequence learning revealed by diffusion magnetic resonance imaging," *Hum Brain Mapp*, vol. 41, no. 2, pp. 442–452, Oct. 2019, doi: 10.1002/hbm.24814.

[3] R. L. Huganir and R. A. Nicoll, "AMPARs and Synaptic Plasticity: The Last 25 Years," *Neuron*, vol. 80, no. 3, pp. 704–717, Oct. 2013, doi: 10.1016/j.neuron.2013.10.025.

[4] P. J. Magistretti, "Neuron–glia metabolic coupling and plasticity," *Journal of Experimental Biology*, vol. 209, no. 12, pp. 2304–2311, Jun. 2006, doi: 10.1242/jeb.02208.

[5] P. Nachev, C. Kennard, and M. Husain, "Functional role of the supplementary and pre-supplementary motor areas," *Nat Rev Neurosci*, vol. 9, no. 11, Art. no. 11, Nov. 2008, doi: 10.1038/nrn2478.

[6] J. S. Erlichman *et al.*, "Inhibition of Monocarboxylate Transporter 2 in the Retrotrapezoid Nucleus in Rats: A Test of the Astrocyte–Neuron Lactate-Shuttle Hypothesis," *J Neurosci*, vol. 28, no. 19, pp. 4888–4896, May 2008, doi: 10.1523/JNEUROSCI.5430-07.2008.

[7] L. C. Mayorquin, A. V. Rodriguez, J.-J. Sutachan, and S. L. Albarracín, "Connexin-Mediated Functional and Metabolic Coupling Between Astrocytes and Neurons," *Frontiers in Molecular Neuroscience*, vol. 11, 2018, Accessed: Dec. 12, 2023. [Online]. Available: https://www.frontiersin.org/articles/10.3389/fnmol.2018.00118

[8] S. Haar and A. A. Faisal, "Brain Activity Reveals Multiple Motor-Learning Mechanisms in a Real-World Task," *Frontiers in Human Neuroscience*, vol. 14, 2020, Accessed: Dec. 12, 2023. [Online]. Available: https://www.frontiersin.org/articles/10.3389/fnhum.2020.00354

[9] B. Thon, "Cognition and motor skill learning," *Annals of Physical and Rehabilitation Medicine*, vol. 58, p. e25, Sep. 2015, doi: 10.1016/j.rehab.2015.07.062.

[10] N. Bolognini, "T004 Cognitive processes of motor behavior revealed by tDCS," *Clinical Neurophysiology*, vol. 128, no. 3, p. e2, Mar. 2017, doi: 10.1016/j.clinph.2016.10.103.

[11] R. Nudo, G. Milliken, W. Jenkins, and M. Merzenich, "Use-dependent alterations of movement representations in primary motor cortex of adult squirrel monkeys," *J Neurosci*, vol. 16, no. 2,

pp. 785–807, Jan. 1996, doi: 10.1523/JNEUROSCI.16-02-00785.1996.

[12] M. Honda, M. P. Deiber, V. Ibáñez, A. Pascual-Leone, P. Zhuang, and M. Hallett, "Dynamic cortical involvement in implicit and explicit motor sequence learning. A PET study," *Brain*, vol. 121 (Pt 11), pp. 2159–2173, Nov. 1998, doi: 10.1093/brain/121.11.2159.

[13] M. Petrides, "Impairments on nonspatial self-ordered and externally ordered working memory tasks after lesions of the mid-dorsal part of the lateral frontal cortex in the monkey," *J Neurosci*, vol. 15, no. 1, pp. 359–375, Jan. 1995, doi: 10.1523/JNEUROSCI.15-01-00359.1995.

[14] P. S. Pohl, J. M. McDowd, D. L. Filion, L. G. Richards, and W. Stiers, "Implicit Learning of a Perceptual-Motor Skill After Stroke," *Physical Therapy*, vol. 81, no. 11, pp. 1780–1789, Nov. 2001, doi: 10.1093/ptj/81.11.1780.

[15] V. Anggono and R. L. Huganir, "Regulation of AMPA Receptor Trafficking and Synaptic Plasticity," *Curr Opin Neurobiol*, vol. 22, no. 3, pp. 461–469, Jun. 2012, doi: 10.1016/j.conb.2011.12.006.

[16] J. A. Lucas, "Memory, Overview," in *Encyclopedia of the Human Brain*, V. S. Ramachandran, Ed., New York: Academic Press, 2002, pp. 817–833. doi: 10.1016/B0-12-227210-2/00198-9.

[17] J.-Y. Hong, E. Gallanter, E. M. Müller-Oehring, and T. Schulte, "Phases of procedural learning and memory: characterisation with perceptual-motor sequence tasks," *J Cogn Psychol (Hove)*, vol. 31, no. 5–6, pp. 543–558, 2019, doi: 10.1080/20445911.2019.1642897.

[18] D. B. Willingham, "A neuropsychological theory of motor skill learning," *Psychological Review*, vol. 105, no. 3, pp. 558–584, 1998, doi: 10.1037/0033-295X.105.3.558.

[19] J. Bo, S. Jennett, and R. D. Seidler, "Working memory capacity correlates with implicit serial reaction time task performance," *Exp Brain Res*, vol. 214, no. 1, pp. 73–81, Sep. 2011, doi: 10.1007/s00221-011-2807-8.

[20] C. Dahms, S. Brodoehl, O. W. Witte, and C. M. Klingner, "The importance of different learning stages for motor sequence learning after stroke," *Hum Brain Mapp*, vol. 41, no. 1, pp. 270–286, Sep. 2019, doi: 10.1002/hbm.24793.

[21] J. Ashe, O. V. Lungu, A. T. Basford, and X. Lu, "Cortical control of motor sequences," *Current Opinion in Neurobiology*, vol. 16, no. 2, pp. 213–221, Apr. 2006, doi: 10.1016/j.conb.2006.03.008.

[22] J. A. G. Lum, G. M. Clark, P. Barhoun, A. T. Hill, C. Hyde, and P. H. Wilson, "Neural basis of implicit motor sequence learning: Modulation of cortical power," *Psychophysiology*, vol. 60,

no. 2, p. e14179, 2023, doi: 10.1111/psyp.14179.

[23] A. Karni *et al.*, "The acquisition of skilled motor performance: Fast and slow experience-driven changes in primary motor cortex," *Proceedings of the National Academy of Sciences*, vol. 95, no. 3, pp. 861–868, Feb. 1998, doi: 10.1073/pnas.95.3.861.

[24] R. von Bernhardi, L. E. Bernhardi, and J. Eugenín, "What Is Neural Plasticity?," in *The Plastic Brain*, R. von Bernhardi, J. Eugenín, and K. J. Muller, Eds., in Advances in Experimental Medicine and Biology. , Cham: Springer International Publishing, 2017, pp. 1–15. doi: 10.1007/978-3-319-62817-2_1.

[25] R. H. Roth, R. H. Cudmore, H. L. Tan, I. Hong, Y. Zhang, and R. L. Huganir, "Cortical Synaptic AMPA Receptor Plasticity during Motor Learning," *Neuron*, vol. 105, no. 5, pp. 895-908.e5, Mar. 2020, doi: 10.1016/j.neuron.2019.12.005.

[26] M. J. Niciu, B. Kelmendi, and G. Sanacora, "Overview of Glutamatergic Neurotransmission in the Nervous System," *Pharmacol Biochem Behav*, vol. 100, no. 4, pp. 656–664, Feb. 2012, doi: 10.1016/j.pbb.2011.08.008.

[27] M. P. Mattson, "Glutamate and Neurotrophic Factors in Neuronal Plasticity and Disease," *Ann N Y Acad Sci*, vol. 1144, pp. 97–112, Nov. 2008, doi: 10.1196/annals.1418.005.

[28] S. Peng, Y. Zhang, J. Zhang, H. Wang, and B. Ren, "Glutamate receptors and signal transduction in learning and memory," *Mol Biol Rep*, vol. 38, no. 1, pp. 453–460, Jan. 2011, doi: 10.1007/s11033-010-0128-9.

[29] S. Konur and A. Ghosh, "Calcium Signaling and the Control of Dendritic Development," *Neuron*, vol. 46, no. 3, pp. 401–405, May 2005, doi: 10.1016/j.neuron.2005.04.022.

[30] K. F. Tolias *et al.*, "The Rac1-GEF Tiam1 Couples the NMDA Receptor to the Activity-Dependent Development of Dendritic Arbors and Spines," *Neuron*, vol. 45, no. 4, pp. 525–538, Feb. 2005, doi: 10.1016/j.neuron.2005.01.024.

[31] L. Pellerin and P. J. Magistretti, "Glutamate uptake into astrocytes stimulates aerobic glycolysis: a mechanism coupling neuronal activity to glucose utilization.," *Proc Natl Acad Sci U S A*, vol. 91, no. 22, pp. 10625–10629, Oct. 1994.

[32] M. H. Hastings, E. S. Maywood, and M. Brancaccio, "Generation of circadian rhythms in the suprachiasmatic nucleus," *Nat Rev Neurosci*, vol. 19, no. 8, Art. no. 8, Aug. 2018, doi: 10.1038/s41583-018-0026-z.

[33] "Treatment of Circadian Rhythm Sleep–Wake Disorders," *Current Neuropharmacology*, vol.

20, no. 6, pp. 1022–1034, Jun. 2022, doi: 10.2174/1570159x19666210907122933.

[34] H. C. Krishnan and L. C. Lyons, “Synchrony and desynchrony in circadian clocks: impacts on learning and memory,” *Learn Mem*, vol. 22, no. 9, pp. 426–437, Sep. 2015, doi: 10.1101/lm.038877.115.

[35] “Circadian Rhythm Disturbances in Mood Disorders: Insights into the Role of the Suprachiasmatic Nucleus.,” *Neural Plasticity*, vol. 2017, pp. 1504507–1504507, Nov. 2017, doi: 10.1155/2017/1504507.

[36] H. Han, J. Dou, Q. Hou, and H. Wang, “Role of Circadian Rhythm and Impact of Circadian Rhythm Disturbance on the Metabolism and Disease,” *Journal of Cardiovascular Pharmacology*, vol. 79, no. 3, p. 254, Mar. 2022, doi: 10.1097/FJC.0000000000001178.

[37] “Circadian Clock Desynchronization and Insulin Resistance,” *International Journal of Environmental Research and Public Health*, vol. 20, no. 1, pp. 29–29, Dec. 2022, doi: 10.3390/ijerph20010029.

[38] X. Yue, “The role of circadian rhythm in breast cancer, lung cancer, and colorectal cancer,” *Highlights in Science, Engineering and Technology*, vol. 54, pp. 181–188, Jul. 2023, doi: 10.54097/hset.v54i.9754.

[39] J. Q. M. Ly *et al.*, “Circadian regulation of human cortical excitability,” *Nat Commun*, vol. 7, p. 11828, Jun. 2016, doi: 10.1038/ncomms11828.

[40] D. Chi-Castañeda and A. Ortega, “Circadian Regulation of Glutamate Transporters,” *Frontiers in Endocrinology*, vol. 9, 2018, Accessed: Dec. 14, 2023. [Online]. Available: https://www.frontiersin.org/articles/10.3389/fendo.2018.00340

[41] M. J. Leone, C. Beaule, L. Marpegan, T. Simon, E. D. Herzog, and D. A. Golombek, “Glial and light-dependent glutamate metabolism in the suprachiasmatic nuclei,” *Chronobiology International*, vol. 32, no. 4, pp. 573–578, Apr. 2015, doi: 10.3109/07420528.2015.1006328.

[42] G. Tononi and C. Cirelli, “Sleep and synaptic homeostasis: a hypothesis,” *Brain Research Bulletin*, vol. 62, no. 2, pp. 143–150, Dec. 2003, doi: 10.1016/j.brainresbull.2003.09.004.

[43] G. Tononi and C. Cirelli, “Sleep function and synaptic homeostasis,” *Sleep Medicine Reviews*, vol. 10, no. 1, pp. 49–62, Feb. 2006, doi: 10.1016/j.smrv.2005.05.002.

[44] L. de Vivo *et al.*, “Ultrastructural evidence for synaptic scaling across the wake/sleep cycle,” *Science*, vol. 355, no. 6324, pp. 507–510, Feb. 2017, doi: 10.1126/science.aah5982.

[45] D. Balduzzi and G. Tononi, “What can neurons do for their brain? Communicate selectivity

with bursts," *Theory Biosci.*, vol. 132, no. 1, pp. 27–39, Mar. 2013, doi: 10.1007/s12064-012-0165-0.

[46] G. Tononi and C. Cirelli, "Sleep and the price of plasticity: from synaptic and cellular homeostasis to memory consolidation and integration," *Neuron*, vol. 81, no. 1, pp. 12–34, Jan. 2014, doi: 10.1016/j.neuron.2013.12.025.

[47] V. V. Vyazovskiy, C. Cirelli, M. Pfister-Genskow, U. Faraguna, and G. Tononi, "Molecular and electrophysiological evidence for net synaptic potentiation in wake and depression in sleep," *Nat Neurosci*, vol. 11, no. 2, Art. no. 2, Feb. 2008, doi: 10.1038/nn2035.

[48] Y. Qin *et al.*, "State-dependent Ras signaling and AMPA receptor trafficking," *Genes Dev*, vol. 19, no. 17, pp. 2000–2015, Sep. 2005, doi: 10.1101/gad.342205.

[49] F. Lanté, J.-C. Toledo-Salas, T. Ondrejcak, M. J. Rowan, and D. Ulrich, "Removal of synaptic Ca^2+-permeable AMPA receptors during sleep," *J Neurosci*, vol. 31, no. 11, pp. 3953–3961, Mar. 2011, doi: 10.1523/JNEUROSCI.3210-10.2011.

[50] H. W. Kessels and R. Malinow, "Synaptic AMPA receptor plasticity and behavior," *Neuron*, vol. 61, no. 3, pp. 340–350, Feb. 2009, doi: 10.1016/j.neuron.2009.01.015.

[51] "Human Cortical Excitability Increases with Time Awake | Cerebral Cortex | Oxford Academic." Accessed: Dec. 14, 2023. [Online]. Available: https://academic.oup.com/cercor/article/23/2/1/283604

[52] E. V. Lubenov and A. G. Siapas, "Decoupling through synchrony in neuronal circuits with propagation delays," *Neuron*, vol. 58, no. 1, pp. 118–131, Apr. 2008, doi: 10.1016/j.neuron.2008.01.036.

[53] V. V. Vyazovskiy *et al.*, "Cortical firing and sleep homeostasis," *Neuron*, vol. 63, no. 6, pp. 865–878, Sep. 2009, doi: 10.1016/j.neuron.2009.08.024.

[54] C. Volk, V. Jaramillo, R. Merki, R. O'Gorman Tuura, and R. Huber, "Diurnal changes in glutamate + glutamine levels of healthy young adults assessed by proton magnetic resonance spectroscopy," *Hum Brain Mapp*, vol. 39, no. 10, pp. 3984–3992, Jun. 2018, doi: 10.1002/hbm.24225.

[55] "Long-Term Homeostasis of Extracellular Glutamate in the Rat Cerebral Cortex across Sleep and Waking States | Journal of Neuroscience." Accessed: Dec. 14, 2023. [Online]. Available: https://www.jneurosci.org/content/29/3/620.short

[56] E. J. Wamsley, "Memory Consolidation during Waking Rest," *Trends Cogn Sci*, vol. 23, no. 3,

pp. 171–173, Mar. 2019, doi: 10.1016/j.tics.2018.12.007.

[57] E. T. Cowan, A. C. Schapiro, J. E. Dunsmoor, and V. P. Murty, “Memory consolidation as an adaptive process,” *Psychon Bull Rev*, vol. 28, no. 6, pp. 1796–1810, Dec. 2021, doi: 10.3758/s13423-021-01978-x.

[58] G. Albouy *et al.*, “Interaction between Hippocampal and Striatal Systems Predicts Subsequent Consolidation of Motor Sequence Memory,” *PLoS One*, vol. 8, no. 3, p. e59490, Mar. 2013, doi: 10.1371/journal.pone.0059490.

[59] B. Rasch and J. Born, “About Sleep’s Role in Memory,” *Physiol Rev*, vol. 93, no. 2, pp. 681–766, Apr. 2013, doi: 10.1152/physrev.00032.2012.

[60] A. Boutin and J. Doyon, “A sleep spindle framework for motor memory consolidation,” *Philos Trans R Soc Lond B Biol Sci*, vol. 375, no. 1799, p. 20190232, May 2020, doi: 10.1098/rstb.2019.0232.

[61] S. Laventure *et al.*, “NREM2 and Sleep Spindles Are Instrumental to the Consolidation of Motor Sequence Memories,” *PLOS Biology*, vol. 14, no. 3, p. e1002429, Mar. 2016, doi: 10.1371/journal.pbio.1002429.

[62] S. Diekelmann and J. Born, “The memory function of sleep,” *Nat Rev Neurosci*, vol. 11, no. 2, Art. no. 2, Feb. 2010, doi: 10.1038/nrn2762.

[63] J. D. Rudoy, J. L. Voss, C. E. Westerberg, and K. A. Paller, “Strengthening Individual Memories by Reactivating them During Sleep,” *Science*, vol. 326, no. 5956, p. 1079, Nov. 2009, doi: 10.1126/science.1179013.

[64] J. O’Neill, B. Pleydell-Bouverie, D. Dupret, and J. Csicsvari, “Play it again: reactivation of waking experience and memory,” *Trends Neurosci*, vol. 33, no. 5, pp. 220–229, May 2010, doi: 10.1016/j.tins.2010.01.006.

[65] M. A. Wilson and B. L. McNaughton, “Reactivation of hippocampal ensemble memories during sleep,” *Science*, vol. 265, no. 5172, pp. 676–679, Jul. 1994, doi: 10.1126/science.8036517.

[66] G. Piantoni, Y. D. Van Der Werf, O. Jensen, and E. J. W. Van Someren, “Memory traces of long-range coordinated oscillations in the sleeping human brain,” *Hum Brain Mapp*, vol. 36, no. 1, pp. 67–84, Jan. 2015, doi: 10.1002/hbm.22613.

[67] M. Schönauer, S. Alizadeh, H. Jamalabadi, A. Abraham, A. Pawlizki, and S. Gais, “Decoding material-specific memory reprocessing during sleep in humans,” *Nat Commun*, vol. 8, p. 15404, May 2017, doi: 10.1038/ncomms15404.

[68] J. G. Klinzing, N. Niethard, and J. Born, “Mechanisms of systems memory consolidation during sleep,” *Nat Neurosci*, vol. 22, no. 10, Art. no. 10, Oct. 2019, doi: 10.1038/s41593-019-0467-3.

[69] J. Born and G. B. Feld, “Sleep to upscale, sleep to downscale: balancing homeostasis and plasticity,” *Neuron*, vol. 75, no. 6, pp. 933–935, Sep. 2012, doi: 10.1016/j.neuron.2012.09.007.

[70] G. Wang, B. Grone, D. Colas, L. Appelbaum, and P. Mourrain, “Synaptic plasticity in sleep: learning, homeostasis, and disease,” *Trends Neurosci*, vol. 34, no. 9, pp. 452–463, Sep. 2011, doi: 10.1016/j.tins.2011.07.005.

[71] W. Li, L. Ma, G. Yang, and W.-B. Gan, “REM sleep selectively prunes and maintains new synapses in development and learning,” *Nat Neurosci*, vol. 20, no. 3, pp. 427–437, Mar. 2017, doi: 10.1038/nn.4479.

[72] G. H. Diering, R. S. Nirujogi, R. H. Roth, P. F. Worley, A. Pandey, and R. L. Huganir, “Homer1a drives homeostatic scaling-down of excitatory synapses during sleep,” *Science*, vol. 355, no. 6324, pp. 511–515, Feb. 2017, doi: 10.1126/science.aai8355.

[73] M. Sandrini, L. G. Cohen, and N. Censor, “Modulating reconsolidation: a link to causal systems-level dynamics of human memories,” *Trends in Cognitive Sciences*, vol. 19, no. 8, pp. 475–482, Aug. 2015, doi: 10.1016/j.tics.2015.06.002.

[74] J. L. C. Lee, K. Nader, and D. Schiller, “An Update on Memory Reconsolidation Updating,” *Trends in Cognitive Sciences*, vol. 21, no. 7, pp. 531–545, Jul. 2017, doi: 10.1016/j.tics.2017.04.006.

[75] P. Fries, “A mechanism for cognitive dynamics: neuronal communication through neuronal coherence,” *Trends Cogn Sci*, vol. 9, no. 10, pp. 474–480, Oct. 2005, doi: 10.1016/j.tics.2005.08.011.

[76] G. Buzsáki and A. Draguhn, “Neuronal oscillations in cortical networks,” *Science*, vol. 304, no. 5679, pp. 1926–1929, Jun. 2004, doi: 10.1126/science.1099745.

[77] M. Steriade, D. A. McCormick, and T. J. Sejnowski, “Thalamocortical oscillations in the sleeping and aroused brain,” *Science*, vol. 262, no. 5134, pp. 679–685, Oct. 1993, doi: 10.1126/science.8235588.

[78] G. G. Knyazev, “Motivation, emotion, and their inhibitory control mirrored in brain oscillations,” *Neuroscience & Biobehavioral Reviews*, vol. 31, no. 3, pp. 377–395, Jan. 2007, doi: 10.1016/j.neubiorev.2006.10.004.

[79] O. Jensen and J. E. Lisman, “Hippocampal sequence-encoding driven by a cortical multi-item

working memory buffer," *Trends Neurosci*, vol. 28, no. 2, pp. 67–72, Feb. 2005, doi: 10.1016/j.tins.2004.12.001.

[80] N. A. Busch, C. Groh-Bordin, H. D. Zimmer, and C. S. Herrmann, "Modes of memory: early electrophysiological markers of repetition suppression and recognition enhancement predict behavioral performance," *Psychophysiology*, vol. 45, no. 1, pp. 25–35, Jan. 2008, doi: 10.1111/j.1469-8986.2007.00607.x.

[81] F. Oppermann, U. Hassler, J. D. Jescheniak, and T. Gruber, "The rapid extraction of gist-early neural correlates of high-level visual processing," *J Cogn Neurosci*, vol. 24, no. 2, pp. 521–529, Feb. 2012, doi: 10.1162/jocn_a_00100.

[82] O. Jensen, J. Kaiser, and J.-P. Lachaux, "Human gamma-frequency oscillations associated with attention and memory," *Trends Neurosci*, vol. 30, no. 7, pp. 317–324, Jul. 2007, doi: 10.1016/j.tins.2007.05.001.

[83] S. Houweling, A. Daffertshofer, B. W. van Dijk, and P. J. Beek, "Neural changes induced by learning a challenging perceptual-motor task," *NeuroImage*, vol. 41, no. 4, pp. 1395–1407, Jul. 2008, doi: 10.1016/j.neuroimage.2008.03.023.

[84] T. W. Boonstra, A. Daffertshofer, M. Breakspear, and P. J. Beek, "Multivariate time-frequency analysis of electromagnetic brain activity during bimanual motor learning," *Neuroimage*, vol. 36, no. 2, pp. 370–377, Jun. 2007, doi: 10.1016/j.neuroimage.2007.03.012.

[85] P. Zhuang, C. Toro, J. Grafman, P. Manganotti, L. Leocani, and M. Hallett, "Event-related desynchronization (ERD) in the alpha frequency during development of implicit and explicit learning," *Electroencephalogr Clin Neurophysiol*, vol. 102, no. 4, pp. 374–381, Apr. 1997, doi: 10.1016/s0013-4694(96)96030-7.

[86] A. K. Engel and P. Fries, "Beta-band oscillations—signalling the status quo?," *Current Opinion in Neurobiology*, vol. 20, no. 2, pp. 156–165, Apr. 2010, doi: 10.1016/j.conb.2010.02.015.

[87] B. Pollok, D. Latz, V. Krause, M. Butz, and A. Schnitzler, "Changes of motor-cortical oscillations associated with motor learning," *Neuroscience*, vol. 275, pp. 47–53, Sep. 2014, doi: 10.1016/j.neuroscience.2014.06.008.

[88] H. Qi, "Post-Movement Beta Rebound Is Related to Movement Connection," *World Journal of Neuroscience*, vol. 12, no. 2, Art. no. 2, Mar. 2022, doi: 10.4236/wjns.2022.122010.

[89] M. T. Jurkiewicz, W. C. Gaetz, A. C. Bostan, and D. Cheyne, "Post-movement beta rebound is generated in motor cortex: Evidence from neuromagnetic recordings," *NeuroImage*, vol. 32,

no. 3, pp. 1281–1289, Sep. 2006, doi: 10.1016/j.neuroimage.2006.06.005.

[90] T. W. Boonstra, A. Daffertshofer, M. Breakspear, and P. J. Beek, "Multivariate time–frequency analysis of electromagnetic brain activity during bimanual motor learning," *NeuroImage*, vol. 36, no. 2, pp. 370–377, Jun. 2007, doi: 10.1016/j.neuroimage.2007.03.012.

[91] J. M. Tognarelli *et al.*, "Magnetic Resonance Spectroscopy: Principles and Techniques: Lessons for Clinicians," *J Clin Exp Hepatol*, vol. 5, no. 4, pp. 320–328, Dec. 2015, doi: 10.1016/j.jceh.2015.10.006.

[92] M. H. Buonocore and R. J. Maddock, "Magnetic resonance spectroscopy of the brain: a review of physical principles and technical methods," *Reviews in the Neurosciences*, vol. 26, no. 6, pp. 609–632, Dec. 2015, doi: 10.1515/revneuro-2015-0010.

[93] J. R. Yager *et al.*, "Proton magnetic resonance spectroscopy in adult cancer patients with delirium," *Psychiatry Res*, vol. 191, no. 2, pp. 128–132, Feb. 2011, doi: 10.1016/j.pscychresns.2010.11.003.

[94] J. W. Pan and R. I. Kuzniecky, "Utility of magnetic resonance spectroscopic imaging for human epilepsy," *Quant Imaging Med Surg*, vol. 5, no. 2, pp. 313–322, Apr. 2015, doi: 10.3978/j.issn.2223-4292.2015.01.03.

[95] M. J. Knight, B. McCann, R. A. Kauppinen, and E. J. Coulthard, "Magnetic Resonance Imaging to Detect Early Molecular and Cellular Changes in Alzheimer's Disease," *Front Aging Neurosci*, vol. 8, p. 139, Jun. 2016, doi: 10.3389/fnagi.2016.00139.

[96] M. Rango *et al.*, "Magnetic resonance spectroscopy in Parkinson's disease and parkinsonian syndromes," *Funct Neurol*, vol. 22, no. 2, pp. 75–79, 2007.

[97] S. Ramadan, A. Lin, and P. Stanwell, "Glutamate and Glutamine: A Review of In Vivo MRS in the Human Brain," *NMR Biomed*, vol. 26, no. 12, p. 10.1002/nbm.3045, Dec. 2013, doi: 10.1002/nbm.3045.

[98] R. Leech and D. J. Sharp, "The role of the posterior cingulate cortex in cognition and disease," *Brain*, vol. 137, no. 1, pp. 12–32, Jan. 2014, doi: 10.1093/brain/awt162.

[99] R. Leech, S. Kamourieh, C. F. Beckmann, and D. J. Sharp, "Fractionating the Default Mode Network: Distinct Contributions of the Ventral and Dorsal Posterior Cingulate Cortex to Cognitive Control," *J Neurosci*, vol. 31, no. 9, pp. 3217–3224, Mar. 2011, doi: 10.1523/JNEUROSCI.5626-10.2011.

[100] P. G. Sämann *et al.*, "Development of the brain's default mode network from wakefulness to

slow wave sleep," *Cereb Cortex*, vol. 21, no. 9, pp. 2082–2093, Sep. 2011, doi: 10.1093/cercor/bhq295.

[101] M. Brienza and O. Mecarelli, "Neurophysiological Basis of EEG," in *Clinical Electroencephalography*, O. Mecarelli, Ed., Cham: Springer International Publishing, 2019, pp. 9–21. doi: 10.1007/978-3-030-04573-9_2.

[102] N. Houmani *et al.*, "Diagnosis of Alzheimer's disease with Electroencephalography in a differential framework," *PLoS One*, vol. 13, no. 3, p. e0193607, Mar. 2018, doi: 10.1371/journal.pone.0193607.

[103] S. Noachtar and J. Rémi, "The role of EEG in epilepsy: a critical review," *Epilepsy Behav*, vol. 15, no. 1, pp. 22–33, May 2009, doi: 10.1016/j.yebeh.2009.02.035.

[104] X.-J. Dai, J. Zhang, Y. Wang, Y. Ma, and K. Shi, "Editorial: EEG and fMRI for Sleep and Sleep Disorders–Mechanisms and Clinical Implications," *Front Neurol*, vol. 12, p. 749620, Sep. 2021, doi: 10.3389/fneur.2021.749620.

[105] M. A. Bell and K. Cuevas, "Using EEG to Study Cognitive Development: Issues and Practices," *J Cogn Dev*, vol. 13, no. 3, pp. 281–294, Jul. 2012, doi: 10.1080/15248372.2012.691143.

[106] M. Balconi and M. E. Vanutelli, "Functional EEG connectivity during competition," *BMC Neuroscience*, vol. 19, no. 1, p. 63, Oct. 2018, doi: 10.1186/s12868-018-0464-6.

[107] J. C. Gore, "Principles and practice of functional MRI of the human brain," *J Clin Invest*, vol. 112, no. 1, pp. 4–9, Jul. 2003, doi: 10.1172/JCI200319010.

[108] P. M. Matthews, G. D. Honey, and E. T. Bullmore, "Applications of fMRI in translational medicine and clinical practice," *Nat Rev Neurosci*, vol. 7, no. 9, Art. no. 9, Sep. 2006, doi: 10.1038/nrn1929.

[109] P. B. Roemer, W. A. Edelstein, C. E. Hayes, S. P. Souza, and O. M. Mueller, "The NMR phased array," *Magnetic Resonance in Medicine*, vol. 16, no. 2, pp. 192–225, 1990, doi: 10.1002/mrm.1910160203.

[110] S. C. N. Hui *et al.*, "Frequency drift in MR spectroscopy at 3T," *NeuroImage*, vol. 241, p. 118430, Nov. 2021, doi: 10.1016/j.neuroimage.2021.118430.

[111] J. Near, R. Edden, C. J. Evans, R. Paquin, A. Harris, and P. Jezzard, "Frequency and Phase Drift Correction of Magnetic Resonance Spectroscopy Data by Spectral Registration in the Time Domain," *Magn Reson Med*, vol. 73, no. 1, pp. 44–50, Jan. 2015, doi: 10.1002/mrm.25094.

[112] R. Bartha, D. j. Drost, R. s. Menon, and P. c. Williamson, “Spectroscopic lineshape correction by QUECC: Combined QUALITY deconvolution and eddy current correction,” *Magnetic Resonance in Medicine*, vol. 44, no. 4, pp. 641–645, 2000, doi: 10.1002/1522-2594(200010)44:4<641::AID-MRM19>3.0.CO;2-G.

[113] U. Klose, “In vivo proton spectroscopy in presence of eddy currents,” *Magn Reson Med*, vol. 14, no. 1, pp. 26–30, Apr. 1990, doi: 10.1002/mrm.1910140104.

[114] T. Laudadio, N. Mastronardi, L. Vanhamme, P. Van Hecke, and S. Van Huffel, “Improved Lanczos algorithms for blackbox MRS data quantitation,” *J Magn Reson*, vol. 157, no. 2, pp. 292–297, Aug. 2002, doi: 10.1006/jmre.2002.2593.

[115] J. Near *et al.*, “Preprocessing, analysis and quantification in single-voxel magnetic resonance spectroscopy: experts’ consensus recommendations,” *NMR in Biomedicine*, vol. 34, no. 5, p. e4257, 2021, doi: 10.1002/nbm.4257.

[116] R. Simpson, G. A. Devenyi, P. Jezzard, T. J. Hennessy, and J. Near, “Advanced processing and simulation of MRS data using the FID appliance (FID-A)—An open source, MATLAB-based toolkit,” *Magnetic Resonance in Medicine*, vol. 77, no. 1, pp. 23–33, 2017, doi: 10.1002/mrm.26091.

[117] W. T. Clarke, C. J. Stagg, and S. Jbabdi, “FSL-MRS: An end-to-end spectroscopy analysis package,” *Magnetic Resonance in Medicine*, vol. 85, no. 6, pp. 2950–2964, 2021, doi: 10.1002/mrm.28630.

[118] S. C. N. Hui *et al.*, “MRSCloud: A cloud-based MRS tool for basis set simulation,” *Magnetic Resonance in Medicine*, vol. 88, no. 5, pp. 1994–2004, 2022, doi: 10.1002/mrm.29370.

[119] D. Steyrl and G. R. Müller-Putz, “Artifacts in EEG of simultaneous EEG-fMRI: pulse artifact remainders in the gradient artifact template are a source of artifact residuals after average artifact subtraction,” *J. Neural Eng.*, vol. 16, no. 1, p. 016011, Dec. 2018, doi: 10.1088/1741-2552/aaec42.

[120] M. Bullock, G. D. Jackson, and D. F. Abbott, “Artifact Reduction in Simultaneous EEG-fMRI: A Systematic Review of Methods and Contemporary Usage,” *Front Neurol*, vol. 12, p. 622719, Mar. 2021, doi: 10.3389/fneur.2021.622719.

[121] F. Tadel, S. Baillet, J. C. Mosher, D. Pantazis, and R. M. Leahy, “Brainstorm: A User-Friendly Application for MEG/EEG Analysis,” *Computational Intelligence and Neuroscience*, vol. 2011, p. e879716, Apr. 2011, doi: 10.1155/2011/879716.

[122] M. Zaitsev, B. Akin, P. LeVan, and B. R. Knowles, “Prospective Motion Correction in Functional MRI,” *Neuroimage*, vol. 154, pp. 33–42, Jul. 2017, doi: 10.1016/j.neuroimage.2016.11.014.

[123] D. B. Parker and Q. R. Razlighi, “The Benefit of Slice Timing Correction in Common fMRI Preprocessing Pipelines,” *Frontiers in Neuroscience*, vol. 13, 2019, Accessed: Dec. 19, 2023. [Online]. Available: https://www.frontiersin.org/articles/10.3389/fnins.2019.00821

[124] C. Studholme, R. T. Constable, and J. S. Duncan, “Accurate alignment of functional EPI data to anatomical MRI using a physics-based distortion model,” *IEEE Transactions on Medical Imaging*, vol. 19, no. 11, pp. 1115–1127, Nov. 2000, doi: 10.1109/42.896788.

[125] J. A. Mumford, R. A. Poldrack, and T. E. Nichols, Eds., “Spatial normalization,” in *Handbook of Functional MRI Data Analysis*, Cambridge: Cambridge University Press, 2011, pp. 53–69. doi: 10.1017/CBO9780511895029.005.

[126] C. Candemir, “Spatial Smoothing Effect on Group-Level Functional Connectivity during Resting and Task-Based fMRI,” *Sensors*, vol. 23, no. 13, Art. no. 13, Jan. 2023, doi: 10.3390/s23135866.

[127] K. R. A. Van Dijk, T. Hedden, A. Venkataraman, K. C. Evans, S. W. Lazar, and R. L. Buckner, “Intrinsic Functional Connectivity As a Tool For Human Connectomics: Theory, Properties, and Optimization,” *J Neurophysiol*, vol. 103, no. 1, pp. 297–321, Jan. 2010, doi: 10.1152/jn.00783.2009.

[128] K. M. Ramachandran and C. P. Tsokos, *Mathematical Statistics with Applications in R*. Academic Press, 2020.

[129] M. E. Raichle, A. M. MacLeod, A. Z. Snyder, W. J. Powers, D. A. Gusnard, and G. L. Shulman, “A default mode of brain function,” *Proceedings of the National Academy of Sciences*, vol. 98, no. 2, pp. 676–682, Jan. 2001, doi: 10.1073/pnas.98.2.676.

[130] C. A. Elverson and M. E. Wilson, “Cortisol: Circadian Rhythm and Response to a Stressor,” *Newborn and Infant Nursing Reviews*, vol. 5, no. 4, pp. 159–169, Dec. 2005, doi: 10.1053/j.nainr.2005.09.002.

[131] G. Treccani *et al.*, “Stress and corticosterone increase the readily releasable pool of glutamate vesicles in synaptic terminals of prefrontal and frontal cortex,” *Mol Psychiatry*, vol. 19, no. 4, Art. no. 4, Apr. 2014, doi: 10.1038/mp.2014.5.

[132] M. Popoli, Z. Yan, B. McEwen, and G. Sanacora, “The stressed synapse: the impact of stress

and glucocorticoids on glutamate transmission," *Nat Rev Neurosci*, vol. 13, no. 1, pp. 22–37, Nov. 2011, doi: 10.1038/nrn3138.

[133] C. Cajochen, K. Kräuchi, and A. Wirz-Justice, "Role of Melatonin in the Regulation of Human Circadian Rhythms and Sleep," *Journal of Neuroendocrinology*, vol. 15, no. 4, pp. 432–437, 2003, doi: 10.1046/j.1365-2826.2003.00989.x.

[134] N. K. Logothetis, J. Pauls, M. Augath, T. Trinath, and A. Oeltermann, "Neurophysiological investigation of the basis of the fMRI signal," *Nature*, vol. 412, no. 6843, Art. no. 6843, Jul. 2001, doi: 10.1038/35084005.

[135] H. Laufs *et al.*, "EEG-correlated fMRI of human alpha activity," *Neuroimage*, vol. 19, no. 4, pp. 1463–1476, Aug. 2003, doi: 10.1016/s1053-8119(03)00286-6.

[136] T. Kodama and Y. Honda, "Acetylcholine and glutamate release during sleep–wakefulness in the pedunculopontine tegmental nucleus and norepinephrine changes regulated by nitric oxide," *Psychiatry and Clinical Neurosciences*, vol. 53, no. 2, pp. 109–111, 1999, doi: 10.1046/j.1440-1819.1999.00543.x.